Synthesis and Solution Behaviour of $CpFe(CO)(PPh_3)[CO(CH_2)_3N(CH_3)_2]$ (FpC_3NMe_2)

by

Diya Geng

A thesis

presented to the University of Waterloo

in fulfillment of the

thesis requirement for the degree of

Master of Science

in

Chemistry (Nanotechnology)

Waterloo, Ontario, Canada, 2017

AUTHOR'S DECLARATION

I hereby declare that I am the sole author of this thesis. This is a true copy of the thesis, including any required final revisions, as accepted by my examiners.

I understand that my thesis may be made electronically available to the public.

Abstract

Metal carbonyl (MC) colloids in water have a wide range of biomedical applications. The Fp-acyl (Fp: $CpFe(CO)_2$) derivatives are one kind of MC molecules that can be synthesized through migration insertion reaction (MIR). The molecules assemble into colloids stabilized by water carbonyl interaction (WCI) due to the presence of highly polarized carbonyl (CO) groups. In this work, a new MC compound, $CpFe(CO)(PPh_3)[CO(CH_2)_3N(CH_3)_2]$ (FpC_3NMe_2) has been synthesized, in which a dimethylamino ($-NMe_2$) group is attached. FpC_3NMe_2 is non-surface active and hydrophobic, but can be hydrated in neutral water. FpC_3NMe_2 assembles in THF/water, but the colloids are unstable and aggregate into crystal-like precipitates. This instability is attributed to the weakened hydrophobic interaction resulting from the hydratable $-NMe_2$ groups. In strong acidic solutions, FpC_3NMe_2 is found to show amphiphilic characteristics due to the high water solubility of the protonated $-NMe_2$ groups.

Acknowledgements

First, I would like to express my sincere gratitude to my supervisor, Dr. Xiaosong Wang, for his patient guidance and invaluable support through these two years.

I would like to thank my committee members, Dr. Juewen Liu and Dr. Derek Schipper for their insightful advice on my research. Special thanks to Dr. Jean Duhamel for being my defence committee and providing suggestions. I would also like to thank Dr. Michael K.C. Tam and his students for providing access to the instruments. Janet Venne and Valerie Goodfellow are acknowledged for their technical support.

I would like to thank Catherine Van Esch, Kim Rawson and Lisa Pokrajac for ensuring that my program progresses smoothly. Meanwhile, I would like to thank Soochow University for providing me with a chance to spend two years at University of Waterloo.

Next, I would like to express my great thanks to all of my group members. I would like to thank Kai Cao for helping improve my lab skills, Heyan Jiang for providing suggestions on synthesis, Dapeng Liu for discussing experiments and creating a cozy office environment, Nimer Murshid and Nicholas Lanigan for sharing ideas about my research, and Zhen Zhang, Liao Peng, Na Zhou and Shaowei Shi for all the lovely moments we have spent together. Special thanks to my friend, Sheng Li for her encouragement during the thesis wring process.

Finally, I would like to express my special appreciation to my parents. Their love is the continuous driving force for me to complete my degree.

Table of Contents

List of Figures

List of Schemes

List of Table

List of Abbreviations

AFM	Atomic force microscopy
ATR-FTIR	Attenuated total reflection-Fourier transform infrared
CO	Carbonyl
CORM	CO releasing molecule
CORM-2	Tricarbonyldichlororuthenium(II) dimer
COSY	Correlation spectroscopy
Cp	Cyclopentadienyl
CWC	Critical water content
DCM	Dichloromethane
DEA	2-(diethylamino)ethyl methacrylate
DLS	Dynamic light scattering
DMA	2-(dimethylamino)ethyl methacrylate
DMSO	Dimethyl sulfoxide
Fp	Cyclopentadienyl dicarbonyl iron; $CpFe(CO)_2$
Fp_2	Cyclopentadienyl iron dicarbonyl dimmer
FpC_6	$CpFe(CO)(PPh_3)[C(O)(CH_2)_5CH_3]$
FpC_3NMe_2	$CpFe(CO)(PPh_3)[CO(CH_2)_3N(CH_3)_2]$
FpC_3P	$CpFe(CO)_2(CH_2)_3PPh_2$
FpK	Cyclopentadienyl dicarbonyliron potassium

FpR	Alkyldicarbonylcyclopentadienyliron
FT-IR	Fourier transform-infrared spectroscopy
IR	Infrared
LCST	Lower critical solution temperature
MC	Metal carbonyl
MIP	Migration insertion polymerization
MIR	Migration insertion reaction
MS	Mass spectrometry
MW	Molecular weight
NMe_2	Dimethylamino
NMR	Nuclear magnetic resonance
OM	Optical microscopy
PDI	Polydispersity index
PDMAEMA	Poly(2-(dimethylamino)ethyl methacrylate
$PFpC_3P$	Poly(cyclopentadienylcarbonyldiphenylphosphinobutanoyliron)
PFpP	Poly(cyclopentadienylcarbonyldiphenylphosphinoalkyliron)
PMMA	Poly(methyl methacrylate)
P(OEGA)	Poly(oligoethylene glycol acrylate)
PPh_3	Triphenylphosphine
PR_3	Phosphine

P(VBGly)	Poly(vinylbenzyl 1-thioglycerol)
P(VBGly-Ru com)	Poly(vinylbenzyl 1-thioglycerol) blocks bearing $Ru(CO)_3Cl$ moieties
QD	Quantum dot
R_h	Hydrodynamic radius
SEM	Scanning electron microscopy
TEM	Transmission electron microscopy
THF	Tetrahydrofuran
UV-vis	Ultraviolet-visible
WCI	Water carbonyl interaction
XRD	X-ray diffraction

1. Introduction

1.1 Metal Carbonyl (MC) Compounds

Metal carbonyl (MC) compounds are coordination organometallic derivatives of carbonyl (CO) ligands with transition metals. They are recognized as useful catalysts, e.g., the molecular electrocatalysts for CO_2 reduction for their excellent efficiency, selectivity and stability.[1-3] They have also been found to be powerful tools in a wide range of biomedical applications, such as drug design due to tunable redox properties of the transition metal centres,[4, 5] imaging of live cells due to the strong CO stretching vibrations between 1800 and 2200 cm^{-1},[6] and CO delivery due to their antimicrobial properties.[7-9]

Water is a special and crucial solvent in biology.[10] However, the poor aqueous solubility of MC compounds has limited their study to the organic media. Therefore, there has been an increasing interest in the water solubilization of organometallic compounds.[11] For example, although various small CO releasing molecules (CORMs) have been explored,[9, 12] the low stability and solubility of CORMs in water (often insoluble) have confined their clinical use.[13] A new kind of CO-releasing polymeric micelles was developed to address this problem. Those micelles were prepared from diblock copolymers containing hydrophilic poly(oligoethylene glycol acrylate) (P(OEGA)) blocks and poly(vinylbenzyl 1-thioglycerol) blocks bearing $Ru(CO)_3Cl$ moieties (P(VBGly-Ru com)).[14] Dynamic light scattering (DLS) analysis of the aqueous solution of this material (10 mg/mL) showed that the size distribution (in number) is lower than 10 nm, suggesting that the polymers are fully dissolved in water. To study the

antibacterial ability of the material, the effect of P(OEGA)-*b*-P(VBGly-Ru com) on *P. aeruginosa* PAO1 viability was studied, and the result was compared with the cases when the bacteria were untreated, or treated with tricarbonyldichlororuthenium(II) dimer (CORM-2) and P(OEGA)-*b*-P(VBGly), as shown in Figure 1.[14] From the figure, the non-CO copolymer P(OEGA)-*b*-P(VBGly) presented no tendency of the inhibition of cell growth, while both CORM-2 and P(OEGA)-*b*-P(VBGly-Ru com) promoted significant decrease in planktonic and biofilm viability, confirming the antibacterial ability of the MC complexes. However, compared with CORM-2, the polymer showed a better ability in the prolonged prevention of planktonic growth and biofilm formation, demonstrating the advantage of polymeric micelles.

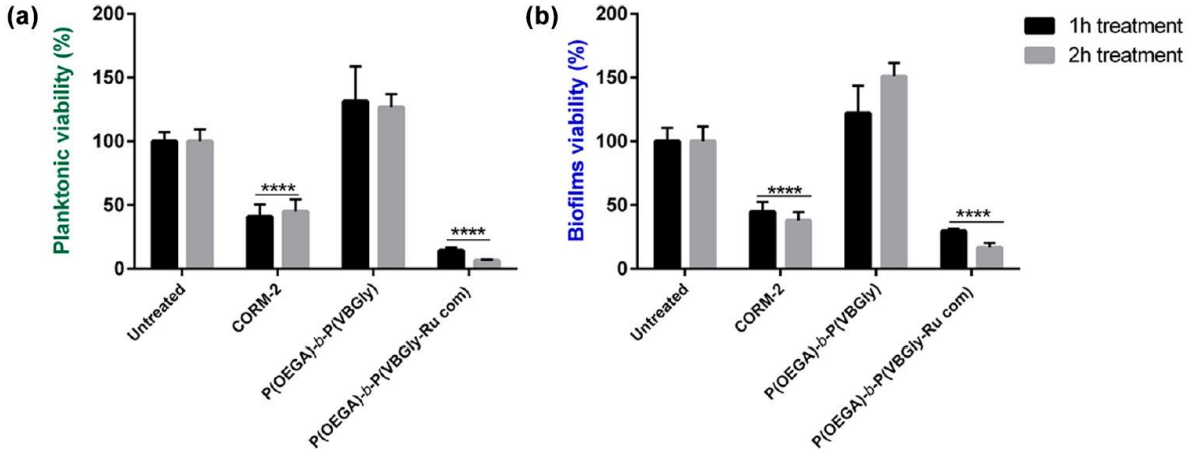

Figure 1. Comparison of (a) planktonic; (b) biofilm viability of *P. aeruginosa* PAO1 when they are untreated, treated with CORM-2, treated with P(OEGA)-*b*-P(VBGly), or treated with P(OEGA)-*b*-P(VBGly-Ru com).[14]

The migration insertion reaction (MIR) has long been studied for the synthesis of organometallic complexes.[15] For instance, as illustrated in Scheme 1, reaction between

alkyldicarbonylcyclopentadienyliron (FpR) and nucleophilic ligands, e.g. phosphine (PR_3), leads to phosphine-coordinated acyl complexes as a result of MIR.[16] During the MIR process, an acyl ligand is formed *via* the combination of one CO and alkyl ligand, and the coordination of the phosphine group with the resultant free orbital on the Fe subsequently takes place. The resulted Fp-acyl (Fp: cyclopentadienyl dicarbonyl iron; $CpFe(CO)_2$) complexes are generally stable,[17-19] making it possible for the study of their solution behaviour.

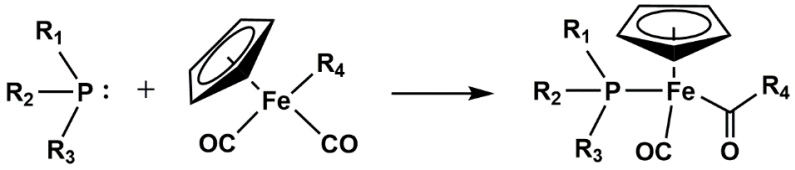

Scheme 1. Schematic illustration of the MIR between FpR and PR_3.

Based on the study of MIR, a new technique called migration insertion polymerization (MIP) has been developed, in which metal complexes act as monomers and join the construction of polymer backbones.[20] The synthesis of the air-stable poly(cyclopentadienylcarbonyldiphenylphosphinobutanoyliron) ($PFpC_3P$) is shown as an example in Scheme 2. The $CpFe(CO)_2(CH_2)_3PPh_2$ (FpC_3P) is prepared *via* a salt-elimination reaction and can be used as a monomer for MIP. At an elevated temperature, FpC_3P undergoes MIP in bulk, resulting in the $PFpC_3P$ with backbone constructed from both P-Fe metal coordination and Fe-C bonds.[21]

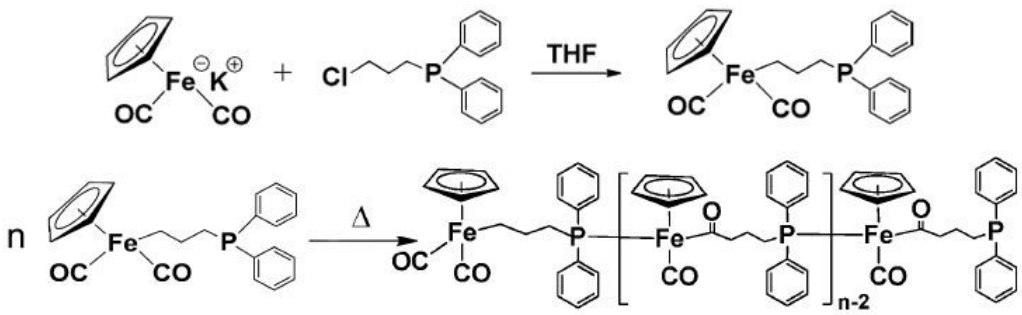

Scheme 2. Synthesis and MIP of FpC_3P.[21]

Poly(cyclopentadienylcarbonyldiphenylphosphinoalkyliron) (PFpP) can function as both positive and negative resists for electron beam lithography. Scanning electron microscopy (SEM) analysis of a line pattern created by using PFpP as a negative resist and tetrahydrofuran (THF) as a developer shows that a line-width as narrow as 16.75 nm can be achieved.[22] This resolution is close to that of the commercially available organic resists. In addition, the presence of metal atoms results in a high beam resistance, which is an advantage for a deep pattern transfer, and is desirable for many applications such as silicon photonics.[23]

1.2 Water Carbonyl Interaction (WCI)

Hydrophobic hydration stands for the direct interaction of hydrophobic molecules with water; hydrophobic interaction is the aggregating principle that prevents hydrophobic surfaces from contacting water, and therefore drives macromolecular assemblies.[24] Hydrophobic hydration has gained substantial attention because of its relevance to biomolecular assembly,[25] such as protein folding[24, 26] and cell membrane formation.[27, 28] Although those biological

macromolecules are hydrophobic and show no obvious amphiphilic features, with a few functional groups interacting with water, they are also able to assemble into a variety of defined structures.[10, 29, 30] The CO group is among those groups that can undergo hydration, and the water carbonyl interaction (WCI) could affect the solution behaviour of some hydrophobic molecules like poly(methyl methacrylate) (PMMA).[31]

The strength of WCI is affected by the polarity of the CO groups.[32] For the MC molecules, the strong electron-donating metal elements can induce negative charges on the oxygen atoms in COs. For example, PFpPs contain highly polarized acyl COs with negative charge density on the oxygen atoms (Figure 2).[33-35] A strong WCI, which is identified to play a crucial role for the aqueous self-assembly of hydrophobic PFpPs, can be exerted by the highly polarized COs. As a result, PFpPs are able to self-assemble into uniform and stable colloids with narrow size distributions in water.[36] This behaviour contradicts common chemical intuition, and proves the possibility that hydrophobic macromolecules could self-assemble into aqueous colloids *via* hydration forces. However, it was still not clear how the WCI contributes to the aqueous self-assembly of these hydrophobic molecules.

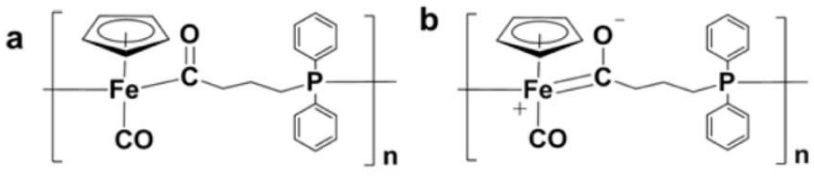

Figure 2. (a) Chemical structure of PFpP; (b) PFpP resonance structure.[36]

The small molecules of the hydrophobic Fp-acyl derivatives, e.g., $CpFe(CO)(PPh_3)[C(O)(CH_2)_5CH_3]$ (FpC_6) and its analogues, have also been reported to be able to self-assemble into vesicles in water.[37, 38] The aqueous self-assembly behaviour of FpC_6 was specially discussed.[37] FpC_6 is hydrophobic and non-surface active. However, due to the WCI caused by acyl and terminal CO groups, the molecules are readily hydrated in water. As shown in Figure 3, by adding water quickly to a THF solution of FpC_6, followed by nitrogen bubbling to remove THF, aqueous FpC_6 colloids were prepared. DLS analysis indicates that the hydrodynamic radius (R_h) of the colloids is 85 nm, with a narrow polydispersity index (PDI) of 0.018. Assumed from the cryo-TEM (TEM: transmission electron microscopy) and the atomic force microscopy (AFM) images, the aggregates are bilayer vesicles with the hydrated Fp-acyl groups exposed towards water, and the hydrophobic alkyl chains forming the inner domain.

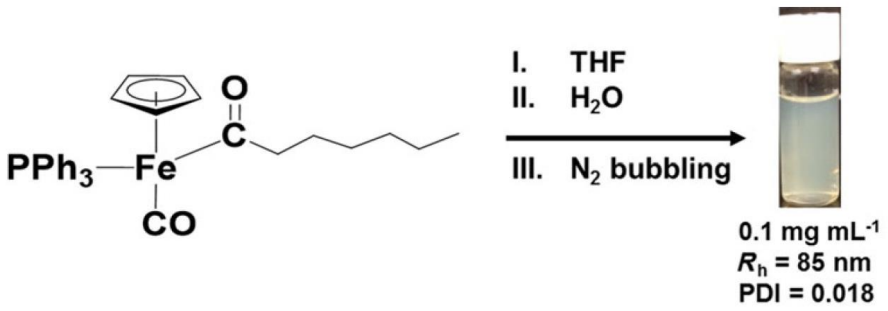

Figure 3. Molecular structure of FpC_6 and its aqueous colloids.[37]

To investigate the effect of WCI on the aqueous self-assembly of FpC_6, both Fourier transform infrared (FT-IR) and DLS analyses were performed on the THF/water solution of FpC_6 as a function of water contents. As shown in Figure 4a, the acyl CO groups have been hydrated

since the initial addition of water, while the terminal CO groups are not hydrated until the water content reaches 60 v% (the degree of FT-IR redshift corresponds to the degree of WCI). DLS results show an increase in count rate at 60 v%, suggesting that the critical water content (CWC) is approximately 60 v% (Figure 4b).[37] Therefore, the terminal CO groups are hydrated after the aggregation starts. Hydrophobic interaction initiates the aggregation, which subsequently induces WCI of the terminal CO, as well as enhances WCI of the acyl CO. When more polarized CO groups pack together, the local electric field is consequently strengthened, which in turn ensures the stability of the aqueous colloids. Therefore, WCI could be responsible for the stability of FpC_6 colloids in water.

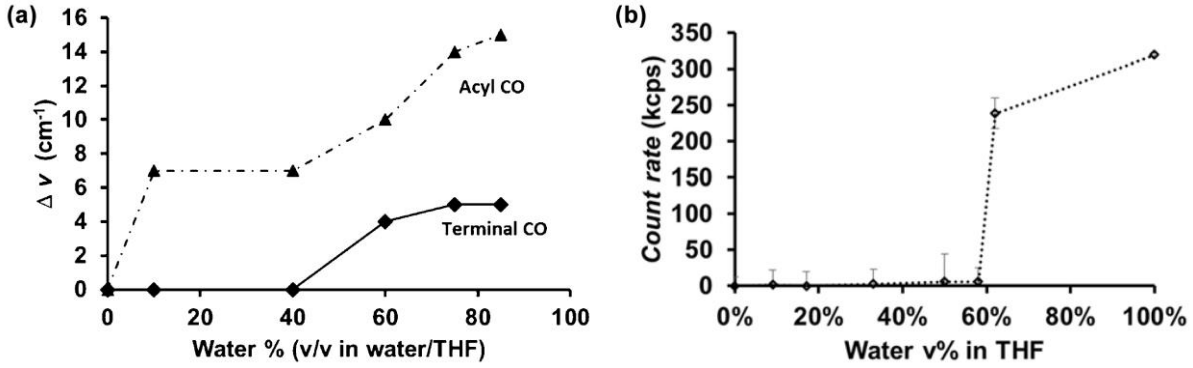

Figure 4. (a) The degree of FT-IR redshift for terminal and acyl CO groups of FpC_6; (b) DLS count rates for FpC_6 in THF/water as a function of water contents.[37]

It has recently been reported that, for the Fp-acyl derivatives, the hydrophobic interaction of alkyl tails is dependent on the assembled structures, and is essential to the stability of the aqueous colloids.[38] In water, the hydrophobic interaction integrates the alkyl chains, while hydration cavities are formed on the surface of the colloids due to the separation of the Fp

heads. Longer alkyl chains result in stronger hydrophobic interaction and larger hydration cavities, and thus greater colloidal stability.[38]

1.3 Dimethylamino (-N(CH_3)$_2$, -NMe_2) Groups

1.3.1 Protonation and Hydration of the -NMe_2 Groups

A dimethylamino (-N(CH_3)$_2$, -NMe_2) group contains a nitrogen atom with a lone pair of electrons,[39] providing the molecules containing these groups with protonation and hydration properties.[40-43] Therefore, functionalization with -NMe_2 groups can be an effective approach to enhancing the solubility of the targeted molecules. For example, the solubility of palladium phthalocyanine (Scheme 3a) is enhanced by the 12 -NMe_2 groups from each molecule. With the tertiary amine substituents, the substance could dissolve in acidic aqueous solutions with a pH lower than 6. After being dissolved in CH_2Cl_2 and stirred with CH_3I at room temperature for 4 hours, the compound became cationic (Scheme 3b), and the quaternized molecules were able to dissolve at all pH values.[44]

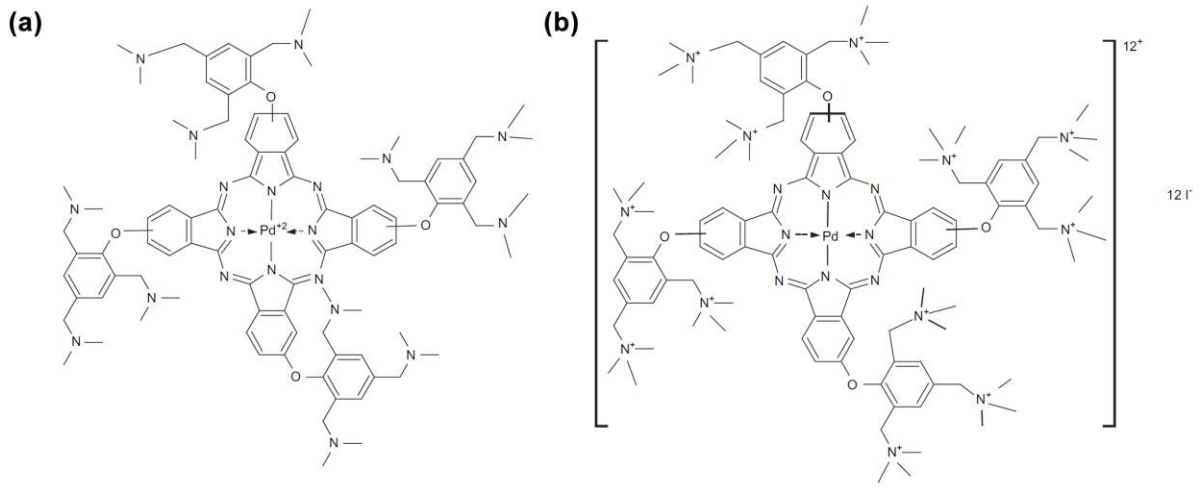

Scheme 3. (a) Tetrakis[2,4,6-tris(N,N-dimethylaminomethyl)phenoxy]phthalocyaninate; (b) Cationic phthalocyanine.[44]

1.3.2 Stimuli-responsive Properties of the -NMe_2 Groups

Stimuli-responsive polymers are high-performance polymers that change properties according to an external stimulus, such as pH value,[45] temperature,[46] light[47] or magnetic field.[48] A number of block copolymers containing the -NMe_2 groups have been found to undergo thermo- or pH-sensitive self-organization into different nanostructures in aqueous solutions.[49-51] Those polymers, which are sensitive to pH or temperature, have wide applications in biological systems, such as drug delivery[52] and gene expression control.[53]

For instance, DMA-DEA (DMA: 2-(dimethylamino)ethyl methacrylate, DEA: 2-(diethylamino)ethyl methacrylate) diblock copolymers undergo pH-induced formation of micelles. These tertiary amine methacrylate copolymers dissolve molecularly in acidic aqueous media, but at pH 7-8, stable block copolymer micelles are formed with hydrophilic

DMA coronas and hydrophobic DEA cores due to deprotonation of both blocks. The R_h value is in the range of 20-60 nm, depending on the block composition. When the pH is lowered, the micelles simply dissolve again (Figure 5).[54]

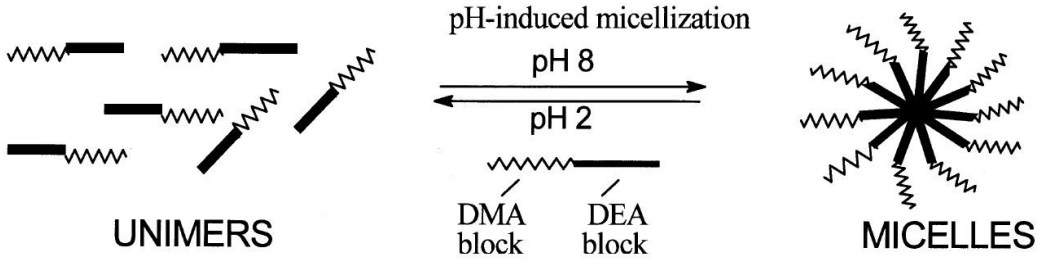

Figure 5. Schematic illustration of pH-induced micellization for DMA-DEA diblock copolymers.[54]

Still based on the properties of DMA, another example is that the PDMAEMA-grafted (PDMAEMA: poly(2-(dimethylamino)ethyl methacrylate) CdTe quantum dots (QDs) can self-assemble into large spheres when the amount of the grafted PDMAEMA is over a certain value. PDMAEMA is a well-known thermal-sensitive polymer that shows a rapid and reversible lower critical solution temperature (LCST) phase transition in water,[55] and the study proves that CdTe QDs are also able to display such a temperature-responsive behaviour after being functionalized with PDMAEMA. The temperature-induced self-assembly mechanism of the QD@PDMAEMA is speculated in Figure 6a, and the TEM images of the molecules at different temperatures are shown in Figure 6b. As illustrated in Figure 6, the polymer dissolves well in water at room temperature. When the temperature gradually approaches the LCST, driven by the effect of the hydrophilic/hydrophobic transition, the PDMAEMA chains slowly shrink, and

network-like intermediate structures are formed. When the temperature is increased above the LCST, the polymer chains completely shrink and collapse, followed by the agglomeration of the small aggregates into large spheres. All of these transformations are reversible. By adjusting the weight fraction of the grafted polymer, the LCST of the QD@PDMAEMAs can be controlled in a range of ca. 32-38 ℃, which is very close to the body temperature (36.5 ± 0.5 ℃), with promising thermo-stimuli biological applications for the smart nanohybrids of QD@PDMAEMAs.[56]

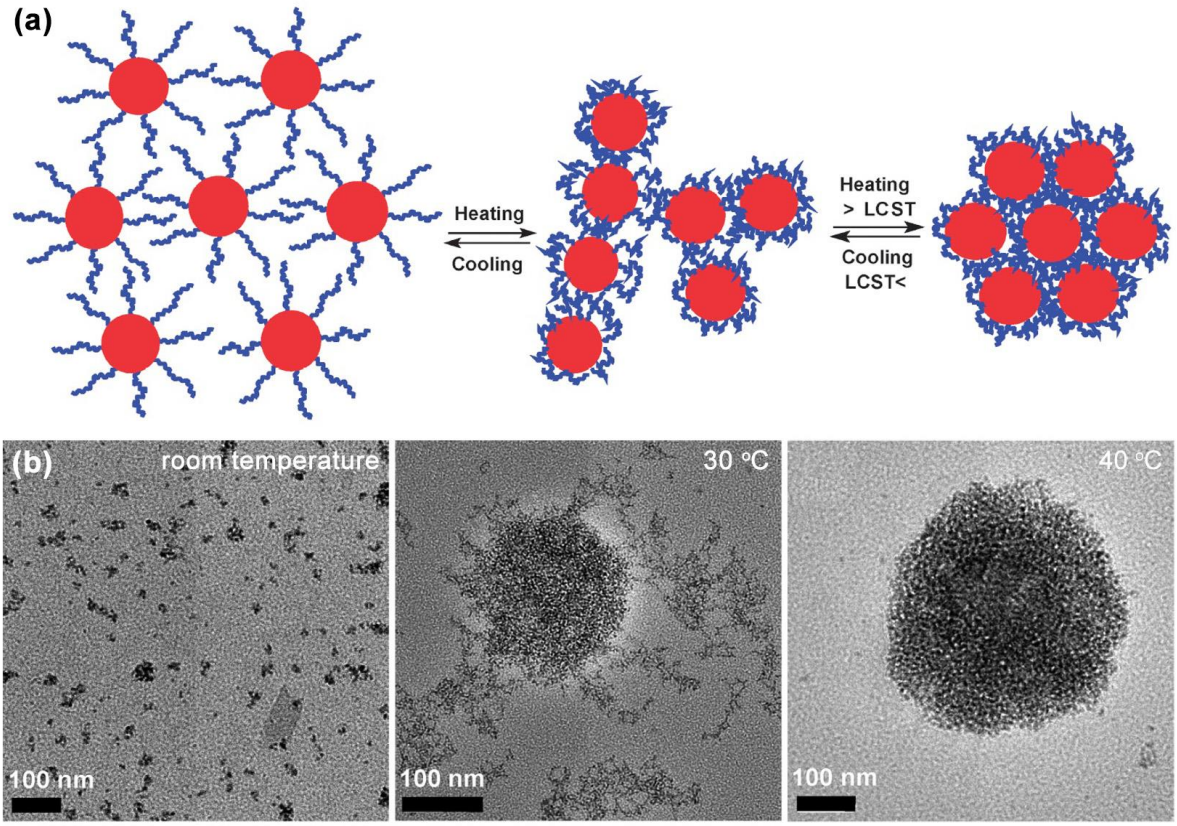

Figure 6. (a) Schematic illustration for the thermally induced aqueous assembly/disassembly process of QD@PDMAEMA; (b) Representative TEM images of one QD@PDMAEMA sample at different temperatures.[56]

1.3.3 Problem Concerning the Purification

Due to the existence of silanol groups (Si-OH) on the surface, silica gel generally exhibits weak acidity.[57] As a result, the -NMe_2 groups with lone pairs of electrons on the nitrogen atoms could be adsorbed on silica particles,[54] complicating the purification of these compounds. There are two possible solutions to this problem. One is to treat the silica gel with trimethylamine prior to use to passivate the weak acidity.[58-60] The other is to purify the acid-sensitive products on neutral alumina instead of silica gel.[61-63]

1.4 Research Goal

This work is centred on one metal carbonyl molecule, $CpFe(CO)(PPh_3)[CO(CH_2)_3N(CH_3)_2]$ (FpC_3NMe_2). With the WCI exerted by the CO groups, and the protonation of the -NMe_2 groups, FpC_3NMe_2 was expected to show some special solution behaviour. It was also expected that the introduction of the -NMe_2 groups could improve the solubility of the Fp-acyl molecules and render them stimuli-responsive. The work presented in this thesis is discussed in the sequence of synthesis, hydration in water and self-assembly behaviour in THF/water mixtures.

2. Experimental

2.1 Materials

All reactions were performed under an atmosphere of dry nitrogen using standard Schlenk techniques unless otherwise indicated. THF was freshly distilled under nitrogen from sodium/benzophenone. Toluene was degassed with dry nitrogen before use. Sodium, potassium, sodium hydroxide (NaOH), sodium chloride (NaCl), anhydrous sodium sulfate (Na_2SO_4), cyclopentadienyl iron(II) dicarbonyl dimer (Fp_2), 3-dimethylamino-1-propyl chloride hydrochloride ($Cl(CH_2)_3NMe_2 \cdot HCl$), trimethylamine, deuterated chloroform ($CDCl_3$) and hydrochloric acid (HCl) were purchased from Sigma-Aldrich. Benzophenone was obtained from Fisher Scientific. Triphenylphosphine (PPh_3) was purchased from Tokyo Chemical Industry. Deuterated benzene (C_6D_6) and dimethyl sulfoxide (DMSO-d_6) were obtained from Cambridge Isotope Laboratories Inc. All chemicals were used as received unless otherwise indicated.

2.2 Instrumentation

2.2.1 Nuclear Magnetic Resonance (NMR) Spectroscopy

^1H, ^{31}P and ^{13}C one dimensional nuclear magnetic resonance (NMR) and ^1H-^1H correlation spectroscopy (COSY) two-dimensional NMR spectra were recorded on a Bruker Advance 300 spectrometer at ambient temperature using appropriate solvents.

2.2.2 Mass Spectrometry (MS)

The mass spectrum was obtained on Thermo Scientific Q-Exactive Orbitrap mass spectrometer.

2.2.3 Dynamic Light Scattering (DLS)

DLS analyses were conducted on a Malvern Zetasizer Nano90 with a laser at 633 nm and a fixed angle of 90°. The operating temperature was 25 ℃ unless otherwise indicated. For THF/water solutions with varied water contents, the samples were prepared by separately adding different amounts of water into a THF solution of FpC_3NMe_2 (1.0 mg/mL, 1.0 mL). Afterwards, a series of DLS data were recorded at different water contents.

2.2.4 Surface Tension

Surface tension measurements were performed on a tensiometer Data Physics DCAT 21system.

2.2.5 Ultraviolet-visible (UV-vis) Spectroscopy

Ultraviolet-visible (UV-vis) absorption spectra were obtained using a Varian (Carey 100 Bio) UV-vis spectrophotometer. A quartz cuvette with a path length of 1 cm was used. Water with the same pH value as the water outside the respective dialysis tube was used as blank.

2.2.6 The pH Measurements

The pH values were measured using a Mettler Toledo SevenCompact pH/ion meter S220.

2.2.7 Optical Microscopy (OM)

Optical microscopy (OM) images were acquired on an inverted Zeiss LSM 510 microscope with a 40× objective. The samples were spotted on a microscope glass for the test.

2.2.8 Transmission Electron Microscopy (TEM)

TEM images were recorded using a Philips CM10 electron microscope (60 kV). The samples were prepared by placing one drop of the solution onto a carbon-coated copper grid (Cu-300CN, Pacific rid Tech), and then the grid was left to dry at ambient temperature.

2.2.9 Fourier Transform Infrared (FT-IR) Spectroscopy

FT-IR spectra were recorded on a Bruker Tensor 27 spectrophotometer in attenuated total reflectance (ATR) mode with a Pike MIRacle accessory equipped with a germanium crystal (Pike Technology). One drop of the solution was placed on the germanium crystal for the test. The infrared (IR) frequency of the THF solution of FpC_3NMe_2 (28.0 mg/mL), which was prepared by dissolving FpC_3NMe_2 (28.0 mg) in THF (1.0 mL) was measured at first. Afterwards, a certain amount of water was successively added to the THF solution, and a series of IR spectra were recorded at different water contents.

2.3 Synthesis of $CpFe(CO)(PPh_3)[CO(CH_2)_3N(CH_3)_2]$ (FpC_3NMe_2)

2.3.1 Neutralization of 3-Dimethylamino-1-propyl Chloride ($Cl(CH_2)_3NMe_2$)

To an aqueous solution of $Cl(CH_2)_3NMe_2 \cdot HCl$ (4.0 g, 25.0 mmol, 5.0 mL distilled water), a solution of NaOH (2.0 g, 50.0 mmol, 5.0 mL distilled water) was added dropwise at room temperature with stirring. The pH of the solution was adjusted to 14, and the mixture was left stirring for 1.5 hours. The organic product was then extracted three times using dichloromethane (DCM) (15.0 mL each). In order to remove water more thoroughly, the residual water in the organic product was extracted with brine (saturated NaCl aqueous solution, 25.0 mL), and the product was dried over anhydrous Na_2SO_4 for 1 hour. After filtration, the solvent was removed using a rotatory evaporator, resulting in a colorless transparent liquid of $Cl(CH_2)_3NMe_2$. Yield: 1.98 g, 65 %. ^{1}H NMR ($CDCl_3$): 3.55 ppm (t, 2H, C***H***$_2$Cl), 2.37 ppm (t, 2H, NC***H***$_2$), 2.19 ppm (s, 6H, N(C***H***$_3$)$_2$), 1.89 ppm (m, 2H, CH_2C***H***$_2CH_2$).

2.3.2 Synthesis of Cyclopentadienyl Dicarbonyliron Potassium (FpK)

The synthesis of cyclopentadienyl dicarbonyliron potassium (FpK) was performed according to the literature.[64] Potassium benzophenone ketyl was prepared by stirring benzophenone (4.92 g, 27.0 mmol) and small cut pieces of potassium (0.98 g, 25.0 mmol) in dry THF (70.0 mL). Upon mixing potassium and benzophenone, the mixture turned blue immediately and was stirred overnight to ensure that the potassium had reacted completely. Then Fp_2 (4.60 g, 13.0 mmol) was added to this solution with vigorous stirring. The deep blue colour of potassium

benzophenone disappeared within several minutes and the solution became reddish-brown in colour with the suspension of organometallic solids. The mixture was stirred for 1 hour. After the reaction, THF was removed using a cannula. The residue was washed using dry toluene three times to remove benzophenone and unreacted dimers. The supernatant was colorless in the last wash and was removed. The residue was dried under vacuum yielding a bright yellow powder (FpK). Yield: 3.69 g, 68 %.

2.3.3 Synthesis of FpC_3NMe_2

$Cl(CH_2)_3N(CH_3)_2$ (1.78 g, 14.6 mmol) was dissolved in 15.0 mL THF. The clear solution was then added dropwise into an orange FpK suspension in THF (2.46 g, 11.4 mmol, 25.0 mL THF), and the mixture was stirred at room temperature. The orange colour gradually turned reddish-brown. After 2 hours, PPh_3 (3.29 g, 12.5 mmol) was added to this suspension, and the mixture was refluxed under stirring at 71 ºC for three days. The THF suspension was then passed through a plug of celite to remove the salt. THF was then removed by rotary evaporation. The resulting reddish-brown oil-like crude product was dissolved in a minimum volume of ethyl acetate and purified using silica gel chromatography. At first, the excess colorless PPh_3 was washed off with ethyl acetate/triethylamine (99:1, v/v). Subsequently, the column was flushed with a THF/triethylamine (99:1, v/v) mixture to collect the orange band. The solvent was then removed by rotary evaporation and the orange product (FpC_3NMe_2) was dried under vacuum for two days to remove the residual solvents. Yield: 3.21 g, 54%. ^{1}H NMR ($CDCl_3$): 7.58-7.43 ppm (t, 6H, meta -$C_6\boldsymbol{H}_5$), 7.43-7.27 ppm (b, 9H, ortho, para -$C_6\boldsymbol{H}_5$), 4.39 ppm (s, 5H,

$C_5\boldsymbol{H}_5$), 2.86 ppm (m, 1H, -COC$\boldsymbol{H}_2$), 2.56 ppm (m, 1H, -COC$\boldsymbol{H}_2$), 2.09 ppm (s, 6H, N(C$\boldsymbol{H}_3$)$_2$), 1.92 ppm (b, 2H, -COCH$_2$CH$_2$C$\boldsymbol{H}_2$), 1.38 ppm (b, 1H, -COCH$_2$C$\boldsymbol{H}_2$), 1.17 ppm (b, 1H, -COCH$_2$C$\boldsymbol{H}_2$). ^{31}P NMR ($CDCl_3$): 76.4 ppm. ^{13}C NMR (DMSO-d_6): 23 ppm (-COCH$_2$$\boldsymbol{C}H_2$), 45 ppm (N($\boldsymbol{C}H_3$)$_2$), 59 ppm (-COCH$_2CH_2$$\boldsymbol{C}H_2$), 63 ppm (-CO$\boldsymbol{C}H_2$), 85 ppm ($\boldsymbol{C}_5H_5$), 128 ppm, 130 ppm, 133 ppm, 136 ppm (-$\boldsymbol{C}_6$H$_5$), 221 ppm (Fe$\boldsymbol{C}$≡O), 272 ppm (Fe$\boldsymbol{C}$OCH$_2$). HRMS-ESI (m/z): [M+H$^+$] calculated for $C_{30}H_{33}O_2NFeP$ 526.15928, found, 526.15935.

2.4 Exploration of the Solution Behaviour of FpC_3NMe_2

2.4.1 Preparation of Acids and Bases

HCl and NaOH were used to adjust the pH of the water solutions.

Acidic solutions: Aqueous HCl (8.2 mL, 37 wt%) was dissolved in 1 L of distilled water, yielding an aqueous solution with a pH value of 1.1 (a). 1.0 mL of solution a was diluted 10 and 100 times separately, yielding two aqueous solutions with a pH value of 2.1 and 3.0 (b), respectively. 1.0 mL of solution b was diluted 10 and 100 times separately, yielding two aqueous solutions with a pH value of 4.2 and 5.3, respectively.

Basic solutions: NaOH (0.1 g) was dissolved in distilled water (250 mL), yielding an aqueous solution with a pH value of 11.8 (c). 1.0 mL of solution c was diluted 100 times, yielding an aqueous solution with a pH value of 10.2.

2.4.2 Analysis of the Solutions at pH 1 with Different Concentrations

In order to generate FpC_3NMe_2 aqueous solutions with a concentration of 0.1 mg/mL, 0.2 mg/mL, 0.3 mg/mL, 0.4 mg/mL, 0.5 mg/mL, and 0.6 mg/mL separately, 25.0 mL of acidic water (pH 1) was directly added into jars that contained 2.5 mg, 5.0 mg, 7.5 mg, 10.0 mg, 12.5 mg, and 15.0 mg of FpC_3NMe_2 solids, respectively. All of the samples were well sonicated for 5 minutes and left standing on the bench overnight. The surface tension and count rate of the clear solutions were then tested, as shown in Figure 20.

2.4.3 Colloid Preparation at Different pH

1.0 mg (unless otherwise indicated) of FpC_3NMe_2 solids were dissolved in 1.0 mL of THF, yielding a clear yellow solution (1.0 mg/mL). To this THF solution, 10.0 mL (for experiments requiring bubbling or dialysis) or 9.0 mL (for DLS measurements) of distilled water with the corresponding pH was quickly injected.

3. Results and Discussion

3.1 Synthesis of FpC_3NMe_2

3.1.1 Neutralization of $Cl(CH_2)_3NMe_2$

$Cl(CH_2)_3NMe_2$ was neutralized before use (Scheme 4). The neutralization was performed in water, followed by extraction with DCM and brine, dried with anhydrous Na_2SO_4 and rotatory evaporation to remove water and dry the reagent.

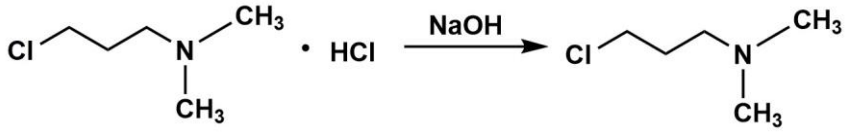

Scheme 4. Neutralization of $Cl(CH_2)_3NMe_2$.

The obtained product is a transparent colorless liquid. The ^1H NMR spectrum is illustrated in Figure 7. As shown in Figure 7, the peak at 2.19 ppm is attributed to the CH_3 groups. The three resonances at 3.55 ppm, 2.37 ppm and 1.89 ppm are due to the CH_2 groups adjacent to the chlorine atom, next to the nitrogen atom, and in the middle of the propyl spacer, respectively.

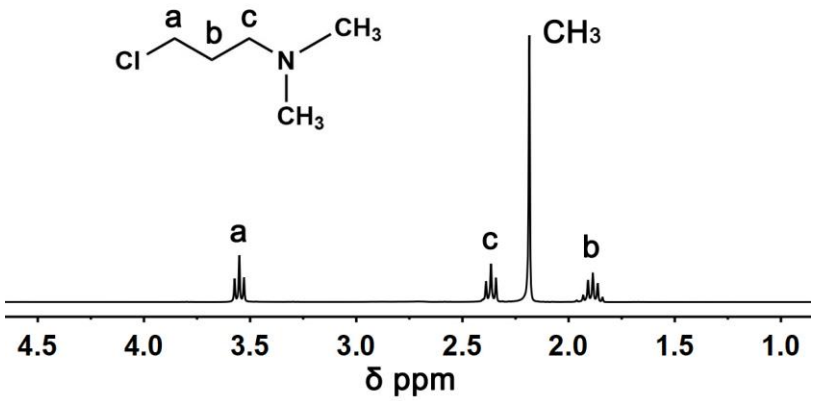

Figure 7. ^{1}H NMR spectrum for $Cl(CH_2)_3NMe_2$ in $CDCl_3$.

3.1.2 Synthesis of FpC_3NMe_2

As shown in Scheme 5, $CpFe(CO)_2(CH_2)_3N(CH_3)_2$ was first prepared *via* a reaction between FpK and $Cl(CH_2)_3NMe_2$ under nitrogen at room temperature. FpC_3NMe_2 was synthesized by the MIR of $CpFe(CO)_2(CH_2)_3N(CH_3)_2$ in the presence of PPh_3 (Scheme 6).

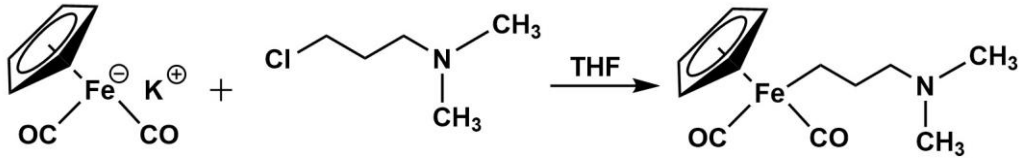

Scheme 5. Synthesis of $CpFe(CO)_2(CH_2)_3N(CH_3)_2$.

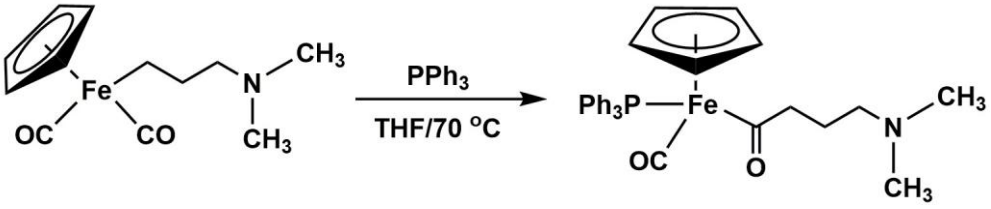

Scheme 6. Synthesis of FpC_3NMe_2.

After purification, a bright orange powder was characterized using ^{31}P NMR, ^{13}C NMR and ^{1}H NMR. As shown in Figure 8, only one peak at 76.4 ppm due to the coordinated phosphorus

appears in the ^{31}P NMR spectrum, which suggests the existence of P-Fe metal coordination. All carbon atoms are assigned in the ^{13}C NMR spectrum (Figure 9), which reveals two signals at 221 ppm and 272 ppm accounting for the terminal and acyl CO groups, respectively.[17] These two peaks prove that the MIR took place successfully. The ^{1}H NMR spectrum is illustrated in Figure 10, which shows two peaks between 7.58-7.43 ppm and 7.43-7.27 ppm due to the meta and ortho/para protons in the phenyl groups, respectively. The peak at 4.39 ppm is assigned to the protons in the cyclopentadienyl (Cp) ring. The resonances at 2.86 ppm and 2.56 ppm correspond to the two diastereotopic protons α to the acyl CO groups.[17] Signal due to the protons of the CH_3 groups is observed at 2.09 ppm. The peak at 1.92 ppm is attributed to the protons in CH_2 adjacent to the nitrogen atom, while the two resonances at 1.38 ppm and 1.17 ppm are assigned to the protons β to the acyl CO groups. The integration ratio for the peaks due to the Cp rings, the phenyl groups and the CH_3 groups is 1 : 3.10 : 1.18, which approximates 1 : 3 : 1.2 and matches the ratio for the targeted molecule. The NMR results confirm the chemical structure of FpC_3NMe_2.

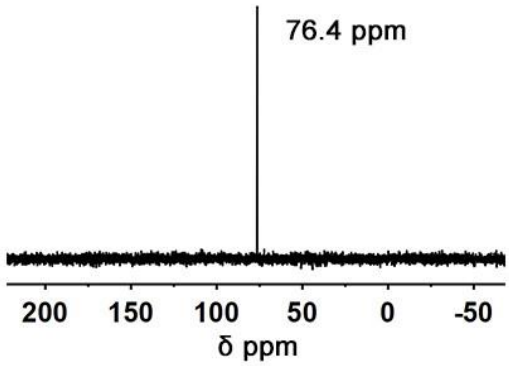

Figure 8. ^{31}P NMR spectrum for FpC_3NMe_2 in $CDCl_3$.

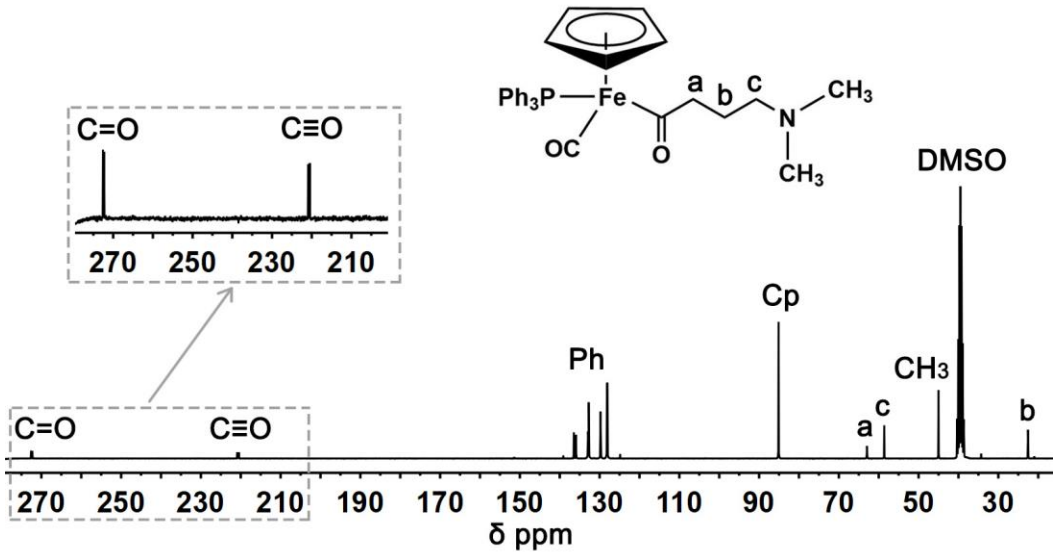

Figure 9. ^{13}C NMR spectrum for FpC_3NMe_2 in DMSO-d_6.

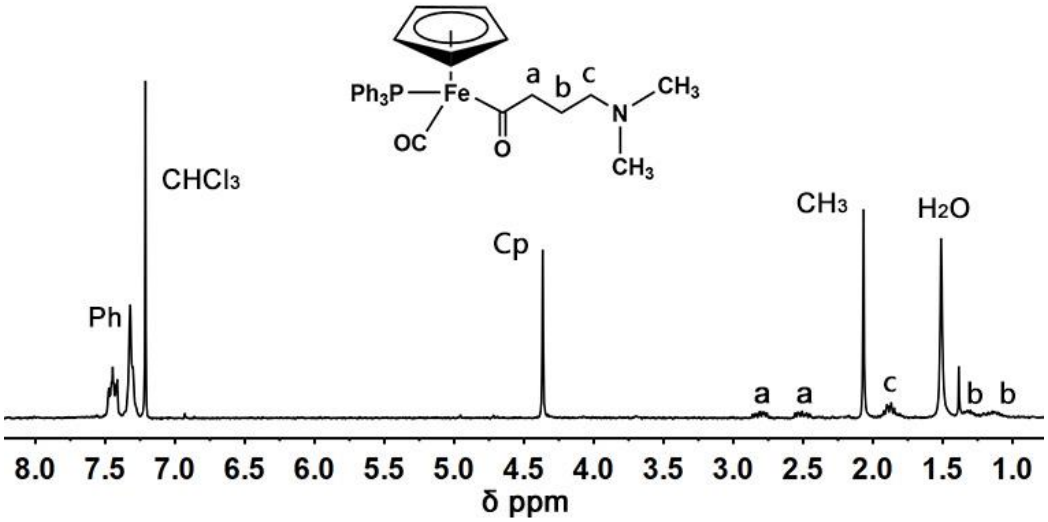

Figure 10. ^{1}H NMR spectrum for FpC_3NMe_2 in $CDCl_3$.

However, in the ^{1}H NMR spectrum, a peak at 1.41 ppm cannot be assigned. As some of the Fp derivatives degrade quickly in $CHCl_3$,[17, 65] ^{1}H NMR analysis was then performed in C_6D_6 and DMSO-d_6. However, the unknown peaks at 1.33 ppm still appear (Figure 11).

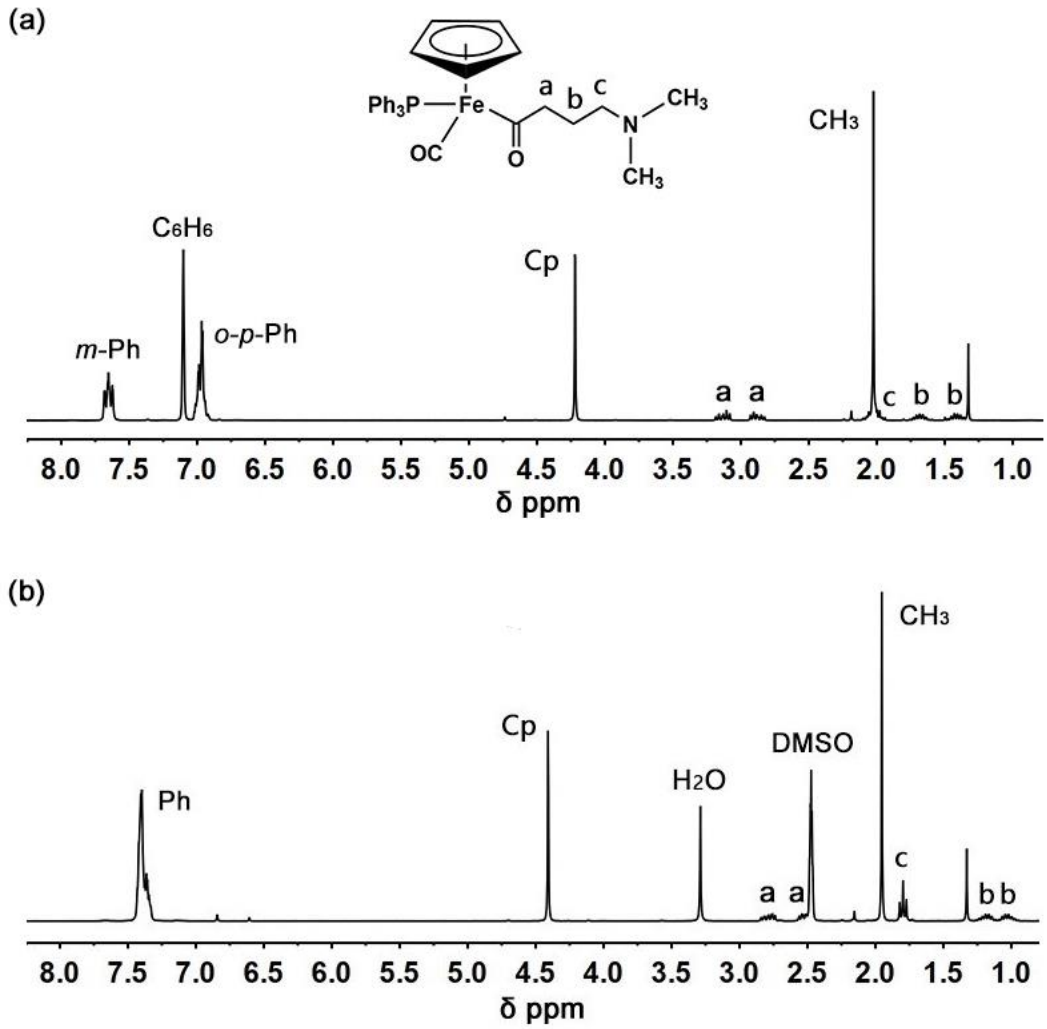

Figure 11. ^{1}H NMR spectrum for FpC_3NMe_2 in (a) C_6D_6; (b) DMSO-d_6.

In order to investigate the unknown peak, and to confirm the assignment of the chemical signals from the protons α and β to the nitrogen atom, ^{1}H-^{1}H COSY 2D NMR was performed. As shown in Figure 12, the chemical shifts at 1.19 ppm and 1.02 ppm correlate to both the triple peaks at 1.81 ppm and the signals from the diastereotopic protons at 2.79 ppm and 2.54 ppm, while no cross peak is observed between the triple peaks (1.81 ppm) and the signals from the diastereotopic protons (2.79 ppm and 2.54 ppm). This correlation proves that the signals at

1.19 ppm and 1.02 ppm are due to the CH_2 protons in the middle of the propyl spacer, which supports the above assignments. No proton signals overlap with the unknown peak at 1.33 ppm, which leads to the conclusion that this peak could not be due to the targeted molecule.

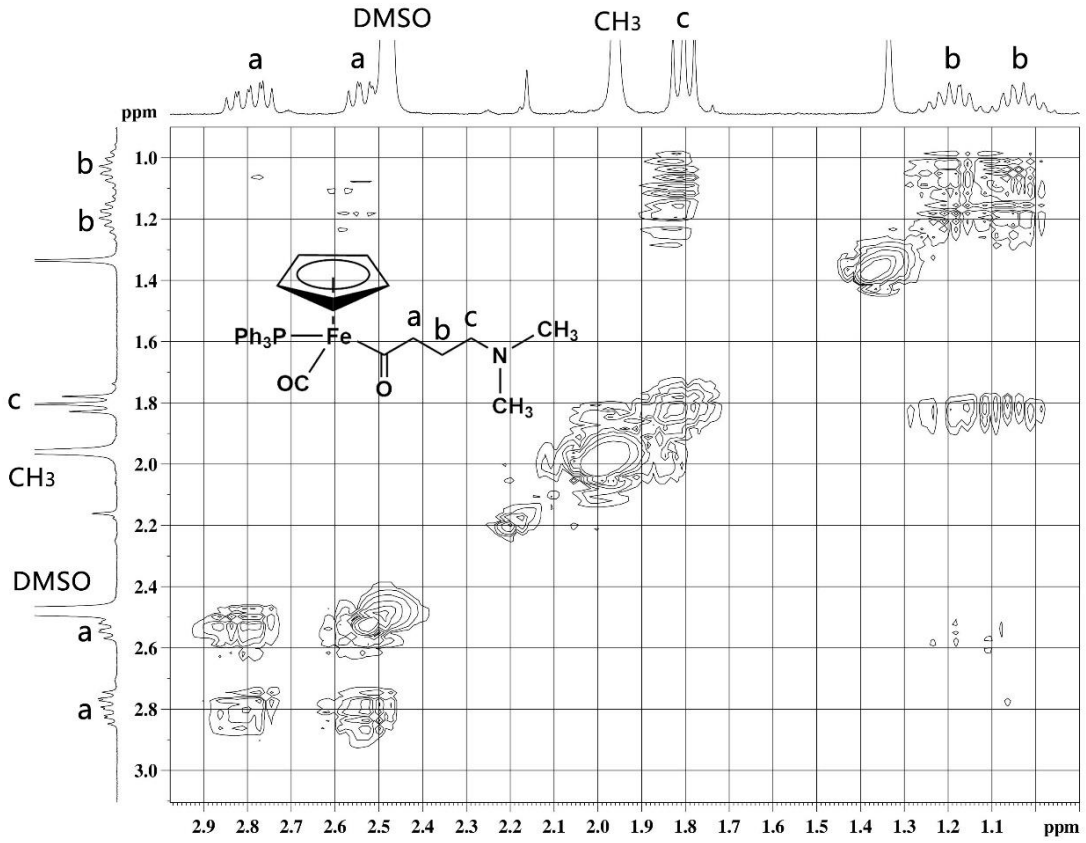

Figure 12. ^1H-^1H COSY 2D NMR spectrum for FpC_3NMe_2 in DMSO-d_6.

MS was applied on the product to support this conclusion, and the spectrum is shown in Figure 13. From the spectrum, the molecular weight (MW) of the protonated product is determined to be 526.15935 g/mol, while the calculated value is 526.15928 g/mol. The slight difference (less than 0.0001 g/mol) indicates that there are no extra atoms in the product molecule, and thus suggests that the unknown peak probably is a solvent impurity. However, in the NMR spectra,

none of the peaks for the involved solvents (THF, toluene, ethyl acetate and trimethylamine) appear at the locations of the unknown signal.[66] Still, the reason for the appearance of this peak is not yet known.

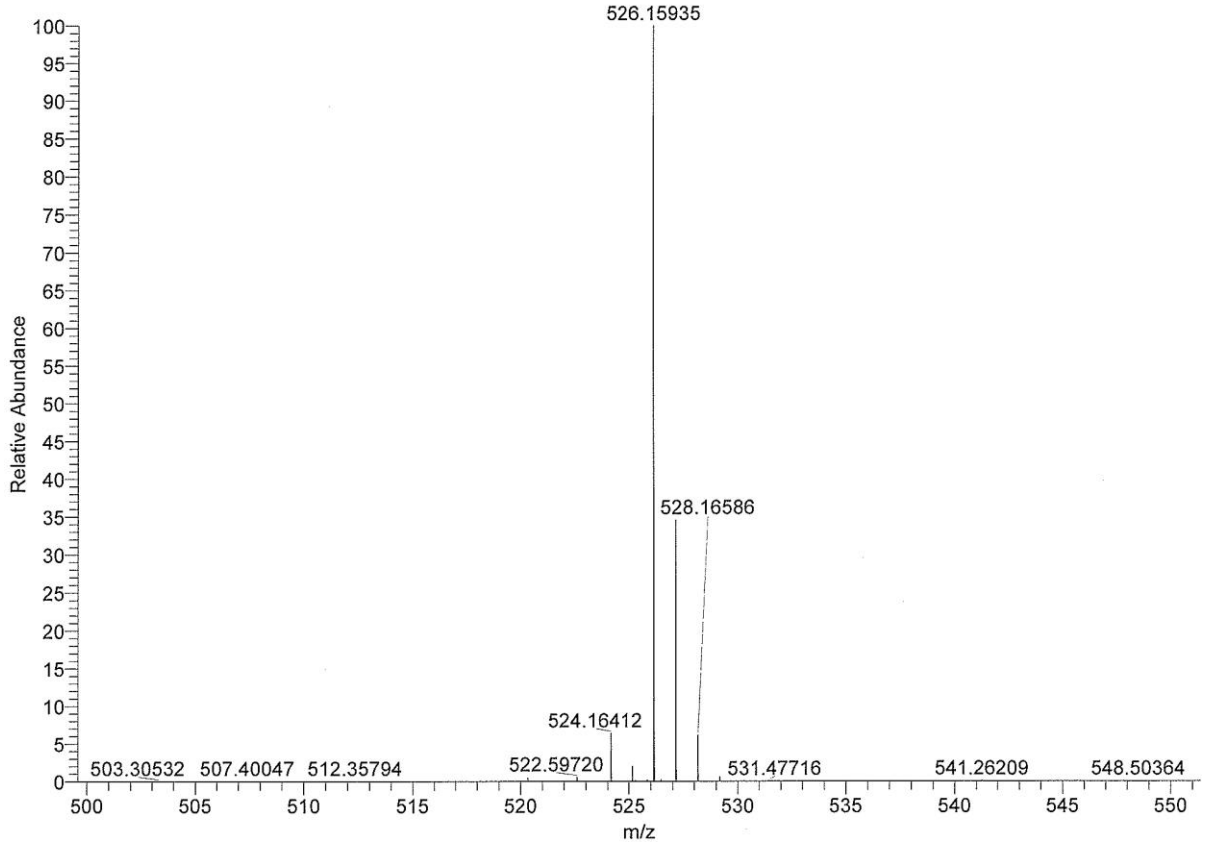

Figure 13. Mass spectrum for FpC_3NMe_2 in acetonitrile.

3.2 Hydrophobic Hydration of FpC_3NMe_2 in Neutral Water

As shown in Figure 14, FpC_3NMe_2 solids either float or sink in water, suggesting that FpC_3NMe_2 is hydrophobic. When 2.0 mg FpC_3NMe_2 was added to 2 L distilled water and stirred overnight, the solution turned light yellow, with solids present at the bottom of the

beaker. DLS analysis shows that the count rate of the solution is only 2.4 kcps, indicating that only a little of the solids is hydrated and suspended in water. The hydrated solid has a R_h of ca. 500 nm with a broad PDI of 1.0. The surface tension of the solution is 72.307 mN/m, which is close to the value of pure water. These results suggest that FpC_3NMe_2 is non-surface active and hydrophobic in neutral water, but can be slightly hydrated.

Figure 14. Hydrophobic FpC_3NMe_2 solids float or sink in water.

To prepare a FpC_3NMe_2 aqueous colloidal solution, 10.0 mL distilled water was quickly added into a THF solution of FpC_3NMe_2 (1.0 mg/mL, 1.0 mL). The resulting solution (0.09 mg/mL) was light yellow upon preparation. Subsequently, dialysis against water was performed to remove THF, resulting in colloids with R_h of 135.0 nm and PDI of 0.131. However, the dialyzed solution was almost colorless, which suggests that substantial FpC_3NMe_2 molecules had diffused through the dialysis membrane. To confirm this hypothesis, a more concentrated colloidal solution (0.9 mg/mL) was prepared and subject to the same dialysis process. During this process, the dialyzate appeared to be slightly yellow with detectable UV-Vis absorption (Figure 15a), confirming that FpC_3NMe_2 molecules had diffused through the membrane. This weak UV-Vis absorbance could be attributed to the transitions between non-bonding orbitals

and pi* orbitals (n→π*) from the carbonyl groups.[67] It is, therefore, possible that there is an equilibrium between the FpC_3NMe_2 assemblies and molecules in water.

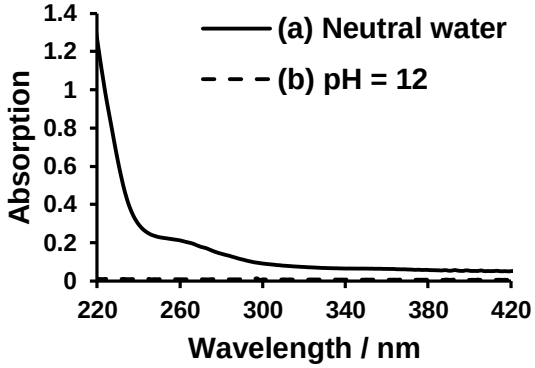

Figure 15. UV-vis spectra for the solution outside the dialysis tube when the initial concentration of the FpC_3NMe_2 colloids was 0.9 mg/mL (a) in neutral water and (b) at pH 12.

As has described in Chapter 1, FpC_6 is a hydrophobic and non-surface active molecule containing a Fp head group, which is similar to FpC_3NMe_2. However, when the colloidal solution of FpC_6 in THF/water (0.09 mg/mL) is dialyzed, the same dialysis process only removes THF, resulting in colloids in water with R_h of ca. 96 nm and PDI of 0.073. This solution behaviour suggests that the integration of FpC_6 colloids in water is stronger than that of FpC_3NMe_2 assemblies, although both molecules are hydrophobic and non-surface active. The lower integration of FpC_3NMe_2 is attributed to the protonation of the amine groups,[68] as illustrated in Scheme 7. To confirm this hypothesis, colloids (0.9 mg/mL) were prepared by adding basic water (pH 12, 10.0 mL) to the THF solution of FpC_3NMe_2 molecules (10.0 mg/mL, 1.0 mL), so that the protonation could be avoided. The dialysis of this solution only

removed THF, and no FpC_3NMe_2 molecules were released into the exterior water as suggested by UV-Vis analysis (Figure 15b).

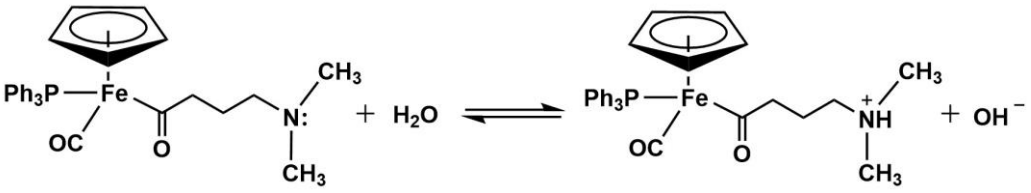

Scheme 7. Protonation of the $-NMe_2$ group of FpC_3NMe_2 in neutral water.

3.3 The Amphiphilic Characteristic of FpC_3NMe_2 in Acid

The $-NMe_2$ groups can be protonated in acidic water and become water-soluble (Scheme 8).[68] It is therefore expected that FpC_3NMe_2 behaves as an amphiphile in an acidic solution.

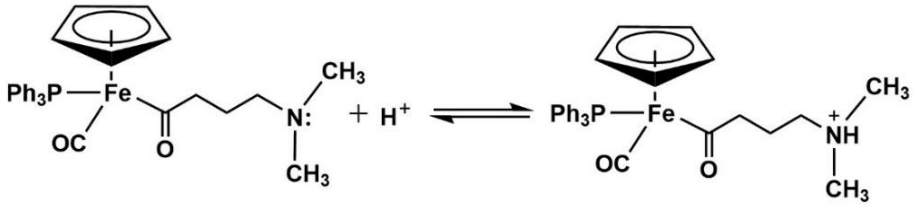

Scheme 8. Protonation of the $-NMe_2$ group of FpC_3NMe_2 in acid.

The solubility of FpC_3NMe_2 in water (1.0 mg/mL) in response to pH was examined first. As shown in Figure 16, when the pH is as high as 5 (Figure 16e), FpC_3NMe_2 solids are obviously insoluble, either floating on the colorless water surface or sinking to the bottom, even after the solution is sonicated. However, yellow suspensions are generated upon sonication of

FpC_3NMe_2 in acidic water (pH lower than 3) due to the protonation of the -NMe_2 groups (Figure 16a-16c).

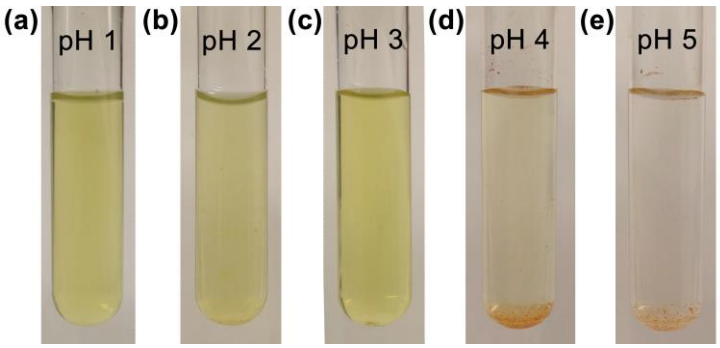

Figure 16. FpC_3NMe_2 aqueous solution (1.0 mg/mL) at pH (a) 1; (b) 2; (c) 3; (d) 4; (e) 5 upon preparation after sonication.

The aqueous behaviour of the solid in water at pH 1 was further investigated. As shown in Figure 17a, upon sonication, the solution of FpC_3NMe_2 (1.0 mg/mL) appears to be homogenous. Gradually, the solution separates into two phases (Figure 17b-17d). The upper layer is colorless and the yellow colour of the lower layer suggests that it is due to flocculated FpC_3NMe_2. After centrifugation, the solid at the bottom of the centrifuge tube is sampled and analyzed by OM, showing that the FpC_3NMe_2 forms aggregates with an average size of 2.58 μm (Figure 18a). Upon drying, the aggregates tend to form films as indicated by the TEM image (Figure 18b).

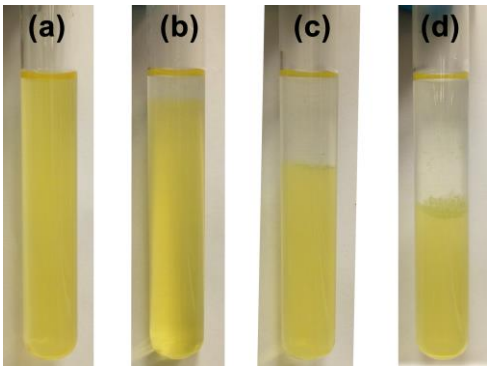

Figure 17. FpC_3NMe_2 aqueous solution (1.0 mg/mL) at pH 1 (a) upon preparation; (b) after 4 hours; (c) after 24 hours; (d) after 48 hours.

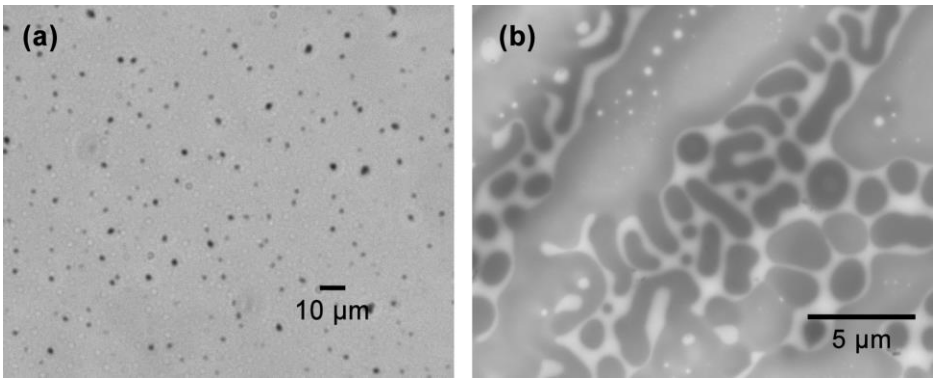

Figure 18. (a) OM (b) TEM image of the FpC_3NMe_2 aggregates recovered from centrifugation of the aqueous solution at pH 1 (1.0 mg/mL).

The flocculated material was recovered *via* centrifugation and the separated wet solid was subsequently dissolved in THF, resulting in a THF/water solution for ^{31}P NMR analysis. As shown in Figure 19b, the spectrum for the recovered material shows one chemical resonance at 76 ppm due to the coordinated phosphorus, and a weak signal appears at 63 ppm as well. When the THF/water solution was left overnight and examined again, the peak at 76 ppm completely converts to the peak at 63 ppm (Figure 19c). Meanwhile, the appearance of a weak

peak at 29 ppm due to oxidized phosphine suggests that a small amount of the molecule has degraded in the THF/water solution.[69]

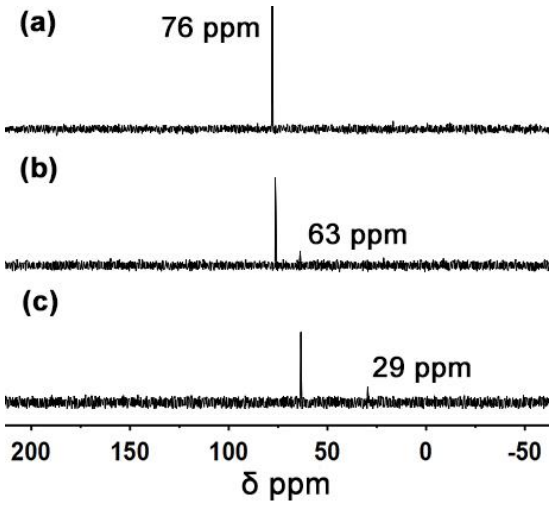

Figure 19. ^{31}P NMR spectrum for (a) the original FpC_3NMe_2; (b) the FpC_3NMe_2 recovered from acid (pH 1) after 2 days and then dissolved in THF; (c) the solution of b being left overnight.

The chemical resonance at 63 ppm is probably the result of the protonation of the acyl CO groups (Scheme 9). In a strong acidic solution, FpC_3NMe_2 molecules are amphiphilic and start to assemble. The assembly is driven by the hydrophobic interaction between the Fp head groups and it is stabilized by the protonated -NMe_2 groups in an acidic environment. The aggregation of the Fp heads segregates them from the acidic water and prevents them from being degraded. However, the protonation of the acyl CO groups becomes possible when the molecules are in an acidic THF/water mixture. Subsequently, the strong acid degrades the metal-containing Fp heads.

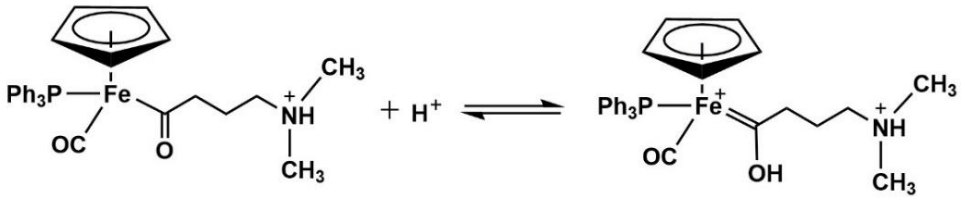

Scheme 9. Protonation of the acyl CO group of FpC_3NMe_2 in acid.

Several solutions at pH 1 with different FpC_3NMe_2 concentrations were prepared by sonication first before leaving them standing overnight. The surface tension of these solutions was measured. As shown in Figure 20, it gradually decreases from 72.3 mN/m, the surface tension of pure water, to ca. 57 mN/m for the solutions with the FpC_3NMe_2 concentration larger than 0.4 mg/mL. From this experiment, 0.4 mg/mL could be considered as the critical aggregation concentration (CAC) for FpC_3NMe_2 in water at pH 1. The degree of the decrease in the surface tension is smaller compared with conventional surfactants,[70] suggesting that the molecule is less surface active.

DLS measurement of the solutions shows that the count rate starts to increase at 0.1 mg/mL (Figure 20), suggesting that the molecules start to aggregate at a concentration much lower than the CAC as indicated by the surface tension experiment. This is attributed to the weaker surface activity of the molecule. When the concentration is 0.6 mg/mL, flocculation is observed in the solution, leading to a sudden drop of the count rate. These results indicate that, although FpC_3NMe_2 presents amphiphilic features, its surface activity is weaker and it behaves differently from conventional surfactants.

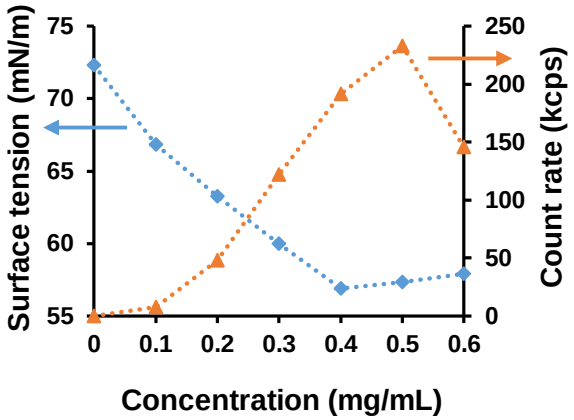

Figure 20. Surface tension and count rate of the aqueous solutions of FpC_3NMe_2 at pH 1 as a function of FpC_3NMe_2 concentration.

3.4 The Self-assembly Behaviour of FpC_3NMe_2 in THF/water

3.4.1 The Instability of FpC_3NMe_2 Colloids in THF/water

The preparation of FpC_3NMe_2 colloids was attempted in water by using the protocol developed for the preparation of FpC_6 aqueous colloids.[37] After 10.0 mL of distilled water was added into the THF solution of FpC_3NMe_2 (1.0 mg/mL, 1.0 mL), THF was subsequently removed by nitrogen bubbling for 1.5 h. However, during the bubbling process, yellow precipitates appeared on the wall of the vial, suggesting that the FpC_3NMe_2 colloids are not stable in water. After the removal of the precipitates, the solution was analyzed by DLS. As illustrated in Figure 21, the R_h of the FpC_3NMe_2 colloids increases dramatically, and the PDI increases to 1.0 after only 10 hours. Correspondingly, irregular particles with varied sizes are observed in the TEM image (Figure 22).

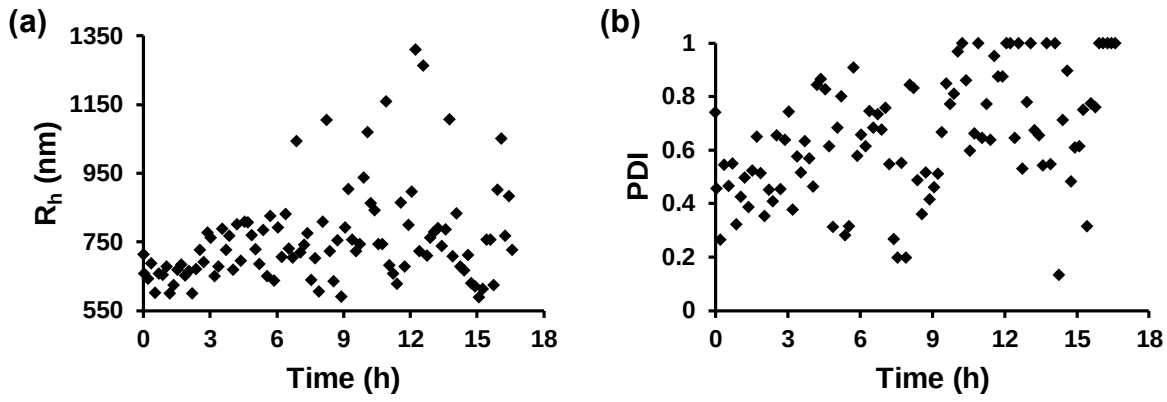

Figure 21. The change of the R_h and PDI of the FpC_3NMe_2 colloids in neutral water after bubbling to remove THF (0.1 mg/mL).

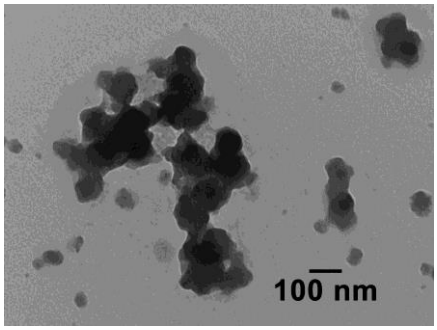

Figure 22. TEM image of the FpC_3NMe_2 colloids in neutral water after bubbling to remove THF (0.1 mg/mL).

The relative stability of FpC_3NMe_2 and FpC_6 colloids in THF/water mixture was compared. As shown in Figure 23, it is clear that both the size and PDI of the FpC_3NMe_2 colloids show a clear upward trend. The R_h of the colloids rises from 196.0 nm to 1085.3 nm, which is more than a fivefold growth. The PDI increases from 0.66 for the freshly prepared sample to 1.0 after about 17 hours. At the same time, the count rate for FpC_3NMe_2 drops from 118.9 kcps to 5.8 kcps (Figure 24), which is in accordance with the phenomenon that FpC_3NMe_2 solids

precipitated after one day. By comparison, FpC_6 colloids show little change during the same period of time. As shown in Figure 23, the R_h of the colloids is still smaller than 100 nm after 20 hours, and the PDI remains smaller than 0.1.

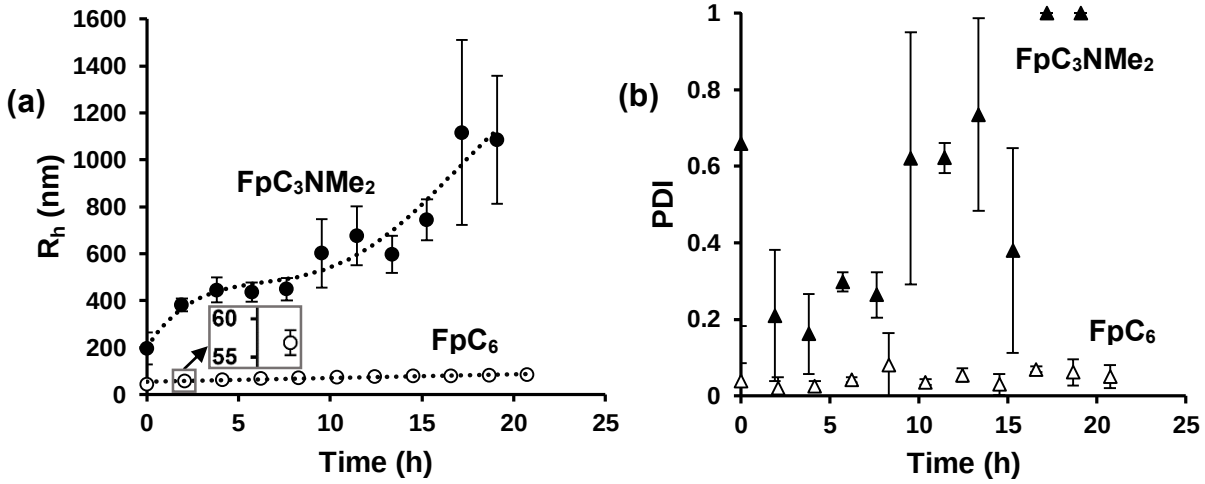

Figure 23. The change of the (a) R_h and (b) PDI of the FpC_3NMe_2 and FpC_6 colloids in THF/water (1:9, v/v) (0.1 mg/mL).

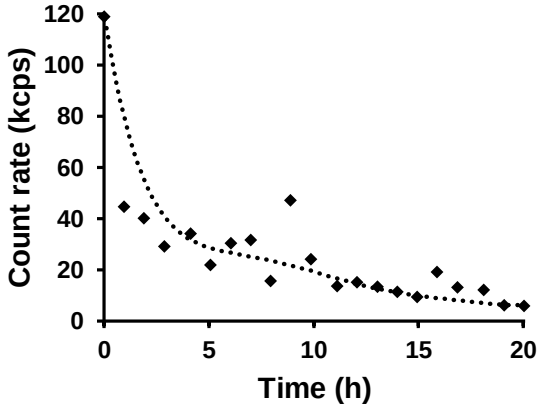

Figure 24. The change of the count rate of the FpC_3NMe_2 colloids in THF/water (1:9, v/v) (0.1 mg/mL).

TEM images for the FpC_3NMe_2 colloidal solution (0.1 mg/mL) are displayed in Figure 25. As shown in Figure 25a, the freshly prepared colloids have various sizes ranging from ca. 350 nm to 1.8 μm, which agrees with the DLS measurements (Figure 23). One day later, after the solids have precipitated, most of the remaining molecules in the solution form small irregular aggregates (Figure 25b).

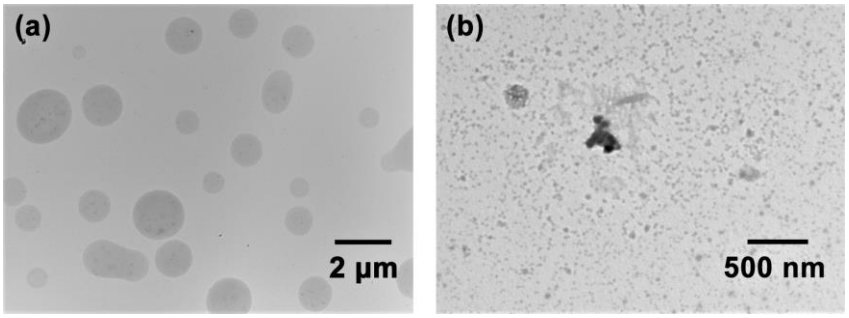

Figure 25. TEM image of the FpC_3NMe_2 colloids prepared at neutral in THF/water (1:9, v/v) (0.1 mg/mL) taken (a) upon preparation; (b) after 1 day.

3.4.2 The Effect of Hydration of -NMe_2 Groups on Colloidal Stability

The reasons for the instability of the FpC_3NMe_2 colloids are worth exploring. Compared with FpC_6, the main difference of FpC_3NMe_2 is the existence of the -NMe_2 groups. It is reasonable to think that the hydration of the -NMe_2 groups contributes to the instability of FpC_3NMe_2 colloids. As was mentioned in Chapter 1, the hydration of -NMe_2 could be constrained in a basic or hot environment. Therefore, in order to suppress the hydration of the -NMe_2 groups, colloids were made in either basic water with a pH value of 12 or in hot water at 65 ºC (0.1 mg/mL). Afterwards, the samples were left at room temperature. The changes in R_h and PDI

of the colloids are shown in Figure 26. As illustrated in Figure 26a, the R_h grows from 61.8 nm to 101.5 nm for the solution with pH 12; while the R_h grows from 146.4 nm to 246.2 nm for the sample prepared at 65 °C. The growth for the both samples levels off after the initial enlargement. The final sizes for both colloids are less than twice the original values, which indicates a much slower growing rate compared to the fivefold increase for the colloids prepared in neutral water at room temperature. As shown in Figure 26b, the lower PDI (lower than 0.2) in these two conditions also supports the relatively higher integration of the FpC_3NMe_2 colloids. This result proves that the instability of the FpC_3NMe_2 colloids prepared in neutral water at room temperature is due to the hydration of the -NMe_2 groups, which weakens the hydrophobic interaction between the tails of the molecules.

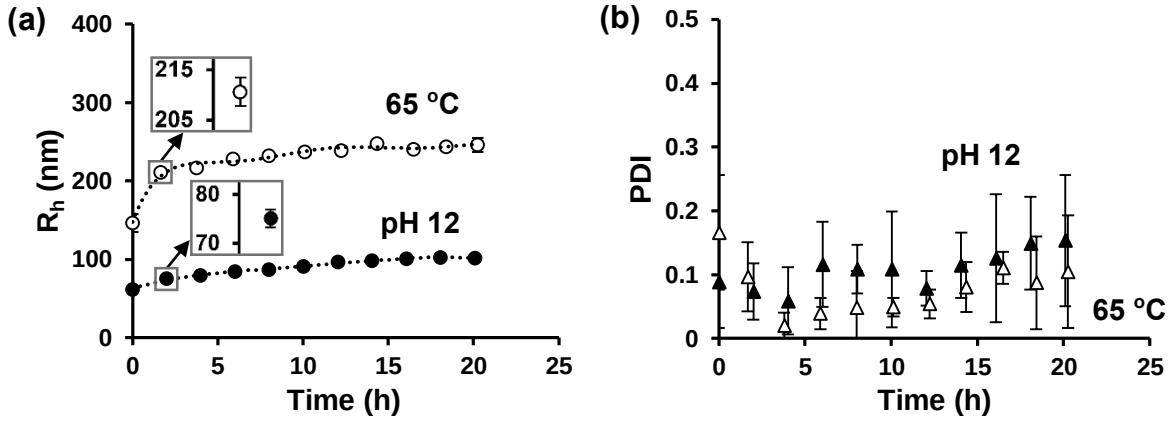

Figure 26. The change of the (a) R_h and (b) PDI of the FpC_3NMe_2 colloids in THF/water (1:9, v/v) (0.1 mg/mL) at pH 12 and 65 °C.

3.4.3 WCI in Response to Water Contents

It has been reported that WCI is responsible for the colloidal stability of FpC_6 assemblies in water.[37] The occurrence of WCI is indicated by IR analysis, which shows the shift of the absorption frequency due to the CO groups towards lower wavenumbers.[71] This attenuated total reflection-Fourier transform infrared (ATR-FTIR) technique was used to investigate the self-assembly of FpC_3NMe_2. Figure 27 lists the IR spectra for the THF/water solutions of FpC_3NMe_2 with increasing amounts of water. When the wavenumbers for the absorption due to the terminal CO (Figure 27a) and the acyl CO groups (Figure 27b) are compared with those in pure THF, the degrees of the shifts in wavenumber ($\Delta\nu$) reveal the degrees of WCI. These data are plotted in Figure 28. As shown in Figure 28, the $\Delta\nu$ for the acyl CO groups is as high as 13 cm^{-1} when the water content is 20 v%, and it keeps increasing when the content reaches 40 v%. The obvious shift indicates that the acyl CO groups can be readily hydrated. However, at the water content of 60 v%, the $\Delta\nu$ for the acyl CO groups suddenly decreases, indicating that the CO groups become dehydrated. For the terminal CO groups, the shift in wavenumber remains nearly unobserved for all the solutions with varied water contents, which suggests that there is no hydration of the terminal CO groups.

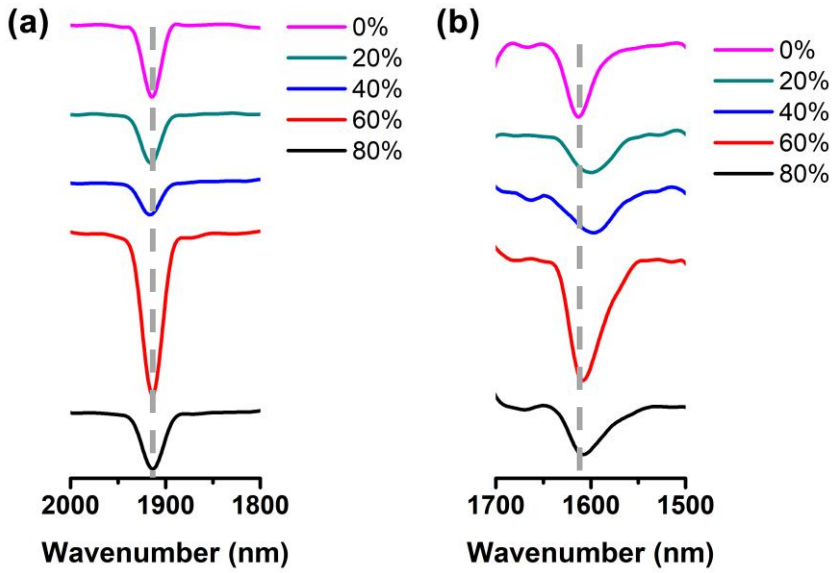

Figure 27. Partial ATR-FTIR spectra for FpC_3NMe_2 in THF/water with varied water contents (28.0 mg/mL at 0 v%, with water successively added).

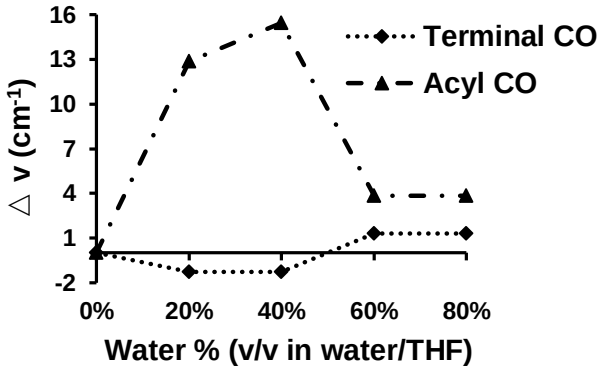

Figure 28. The degree of FT-IR redshift for terminal and acyl CO groups of FpC_3NMe_2 in THF/water as a function of water contents (28.0 mg/mL at 0 v%, with water successively added).

Figure 29 illustrates the DLS analysis results of the solutions with varied amounts of water. As shown in Figure 29a, a substantial increase in count rate is observed when the water content reaches 60 v%, which suggests that aggregation has started. The upsurge in R_h (in number) at

60 v% (Figure 29b) also supports the occurrence of aggregation. It is, therefore, reasonable to claim that the dehydration of the acyl CO groups results from the aggregation. Unlike FpC_3NMe_2, the aggregation of FpC_6 at the CWC (ca. 60 v%) generates a local electric field, which enhances the WCI of the acyl CO groups and initiates the hydration of the terminal CO groups.[37] This comparison suggests that the aggregation of FpC_3NMe_2 is not able to create the local electric field, probably for the reason that the weaker hydrophobic interaction between the tails result in less regular packing of the polarized Fp heads.

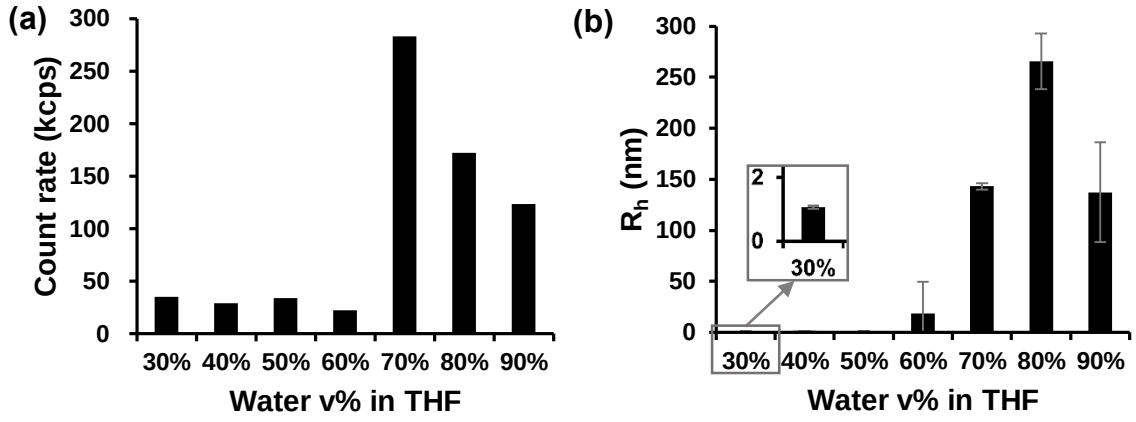

Figure 29. (a) Count rate; (b) R_h of the FpC_3NMe_2 colloids in THF/water as a function of water contents (with varied concentration, from 1.0 mg/mL to 0.1 mg/mL).

3.5 The Solution Behaviour of FpC_3NMe_2 in THF/water at Different pH

The colloidal behaviour of FpC_3NMe_2 (0.1 mg/mL) in THF/water at different pH was studied. The solutions were prepared by adding 9.0 mL distilled water with different pH into a THF solution of FpC_3NMe_2 (1.0 mg/mL, 1.0 mL). Photographs for the solutions upon preparation

are shown in Figure 30. The acidic solutions are almost clear (Figure 30a and 30b), while the neutral and basic solutions are nontransparent, and the transparency decreases with the increase in pH (Figure 30c-30e).

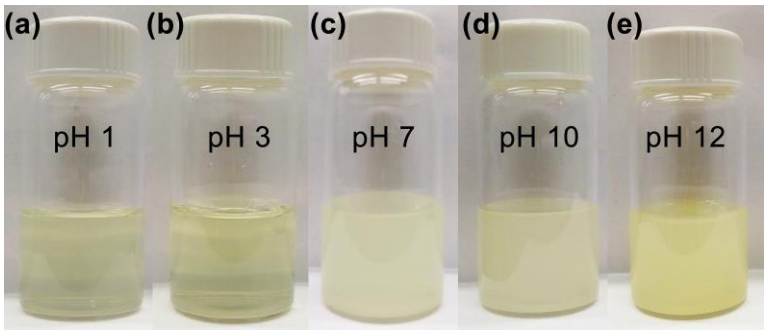

Figure 30. FpC_3NMe_2 colloidal solutions in THF/water (1:9, v/v) (0.1 mg/mL) at pH (a) 1; (b) 3; (c) 7; (d) 10; (e) 12 upon preparation.

The photographs for the solutions aged for one week are shown in Figure 31. As shown in Figure 31, the acidic solutions remain transparent, but the light yellow colour fades to nearly colorless (Figure 31a and 31b). Yellow precipitates at the bottom could be observed for the solutions with pH 7 and higher. In the solution with pH 7, the precipitate appears as a rigid layer (Figure 31c). Small crystal-like precipitates are formed in the solutions with pH 10 and 12 (Figure 31d and 31e) and the crystal-like precipitates are relatively larger in the solution with higher pH.

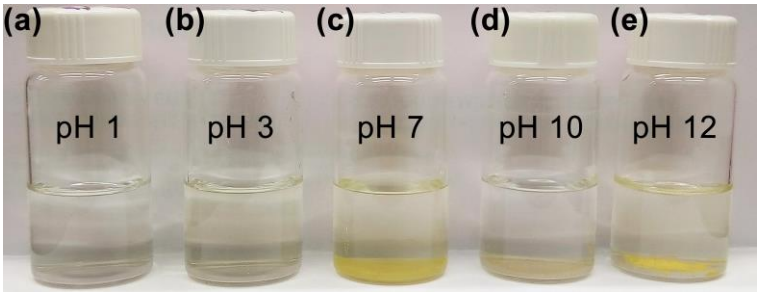

Figure 31. FpC_3NMe_2 colloidal solutions in THF/water (1:9, v/v) (0.1 mg/mL) at pH (a) 1; (b) 3; (c) 7; (d) 10; (e) 12 after being prepared for one week.

3.5.1 The Solution Behaviour in Acidic Environments

The DLS technique was applied to track the R_h and PDI of the FpC_3NMe_2 colloids in the THF/water solutions with pH 1 and 3. As shown in Figure 32, the colloids grow much faster at pH 1 than at pH 3. At pH 1, the R_h of the colloids increases from 68.0 nm to 274.8 nm, which is about a fourfold growth; while at pH 3, the size is close to unchanged during the first five hours, indicating the relative stability of the colloids. The PDIs for the both solutions show substantial divergence, suggesting the irregular formation of the colloids (Figure 33).

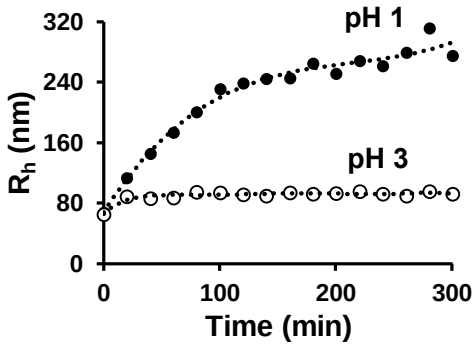

Figure 32. The change of the R_h of the FpC_3NMe_2 colloids in THF/water (1:9, v/v) (0.1 mg/mL) in the first 5 hours at pH 1 and 3.

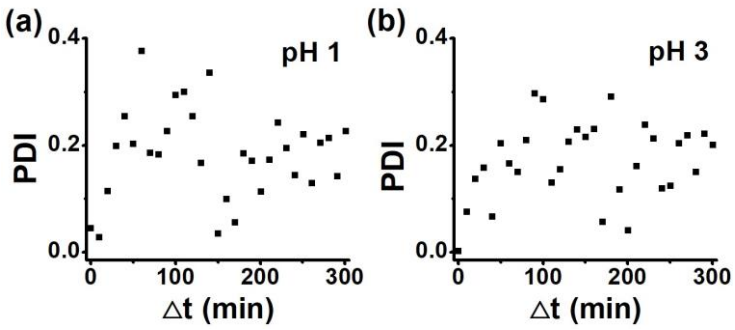

Figure 33. The change of the PDI of the FpC_3NMe_2 colloids in THF/water (1:9, v/v) (0.1 mg/mL) in the first 5 hours at (a) pH 1; (b) pH 3.

Time-resolved ^{31}P NMR spectra of the solutions (1.4 mg/mL) are displayed in Figure 34. As shown in Figure 34a, apart from the peak due to the P-Fe coordination (74 ppm), the chemical resonance at 63 ppm due to the protonation of the acyl CO groups (Chapter 3.4) appears shortly after the solution at pH 1 was prepared. One day later, the peak at 74 ppm disappears. Meanwhile, the intensity of the peak at 63 ppm becomes high before gradually weakening and disappearing over 5 days, suggesting the degradation of the Fp heads (Figure 34a). The precipitates were observed at the bottom of the NMR tube (Figure 35a). For the solution prepared at pH 3, it takes two days for the disappearance of the peak at 74 ppm (Figure 34b) and precipitates were observed as well (Figure 35b). These results suggest that the Fp heads at pH 1 and 3 are chemically unstable and the lower the pH, the faster the degradation.

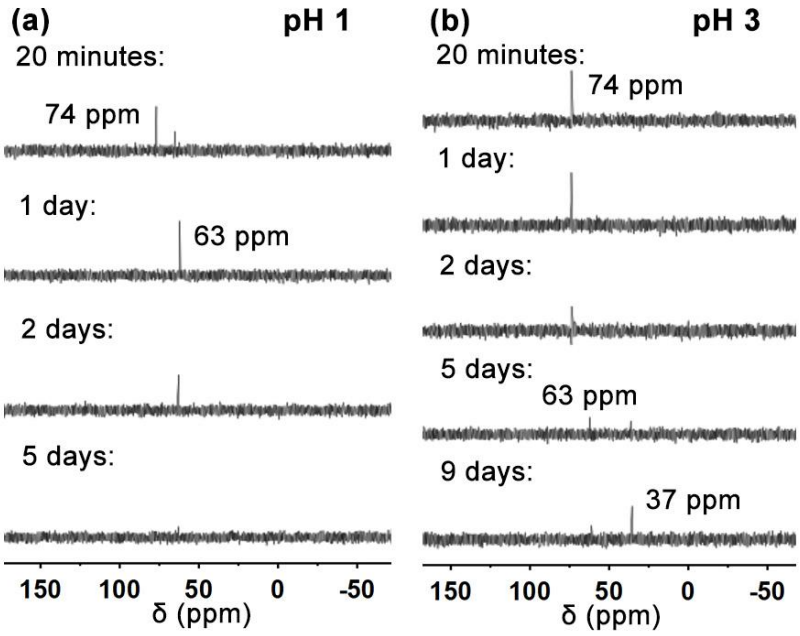

Figure 34. Time-resolved ^{31}P NMR spectra for the THF/water (1:9, v/v) solution of FpC_3NMe_2 at (a) pH 1; (b) pH 3.

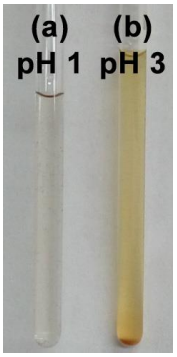

Figure 35. The THF/water (1:9, v/v) solution of FpC_3NMe_2 (1.4 mg/mL) at (a) pH 1; (b) pH 3 (5 days).

TEM images for the solution at pH 3 (0.1 mg/mL) are displayed in Figure 36. As shown in Figure 36a, colloids are freshly prepared and show relatively uniform aggregates with 150 nm

in size, which is consistent with the DLS measurement (Figure 32). Two days later, upon the degradation of the Fp heads, the colloids evolve into very thin lamellae (Figure 36b).

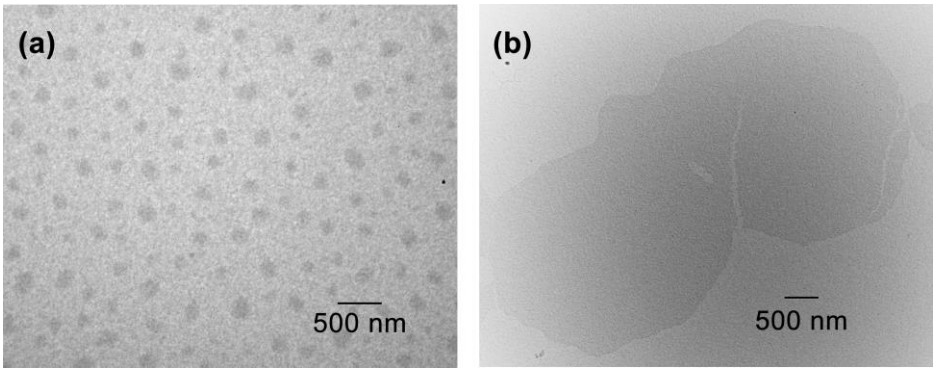

Figure 36. TEM image of the FpC_3NMe_2 colloids prepared in THF/water (1:9, v/v) at pH 3 (0.1 mg/mL) taken (a) upon preparation; (b) after 2 days since preparation.

3.5.2 The Solution Behaviour in Basic and Neutral Environments

OM images for the crystal-like precipitates formed in the basic THF/water solutions are displayed in Figure 37a (pH 12) and Figure 38a (pH 10), indicating that the precipitates have a flat rhombic crystal structure. The presence of materials with very poor crystallinity is confirmed in the TEM image of the upper solution at pH 12 (Figure 37b); while at pH 10, the TEM image of the upper solution shows large amounts of nanoparticles during the nucleation phase (Figure 38b). These two images suggest that the crystallization still took place slowly in the basic solutions.[72, 73]

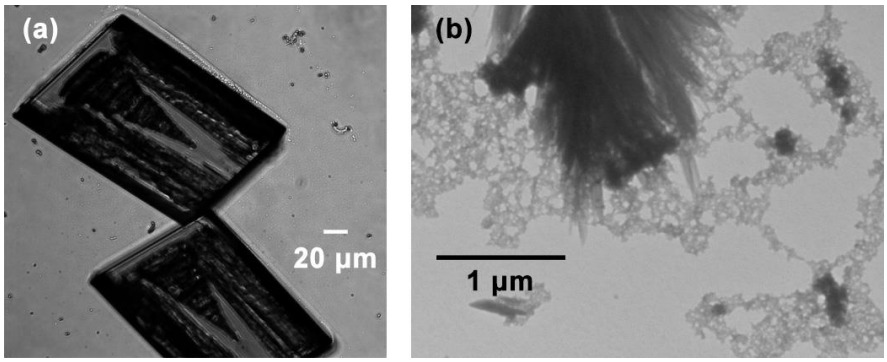

Figure 37. (a) OM image of the FpC_3NMe_2 precipitates prepared in THF/water (1:9, v/v) at pH 12 (0.1 mg/mL) one week after preparation; (b) TEM image of the FpC_3NMe_2 solutions prepared in THF/water (1:9, v/v) at pH 12 (0.1 mg/mL) one week after preparation.

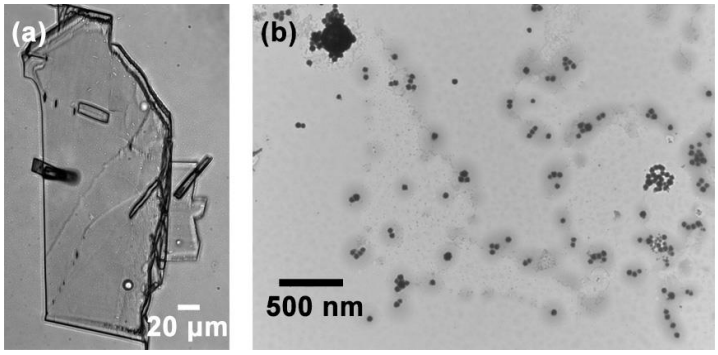

Figure 38. (a) OM image of the FpC_3NMe_2 precipitates prepared in THF/water (1:9, v/v) at pH 10 (0.1 mg/mL) one week after preparation; (b) TEM image of the FpC_3NMe_2 solutions prepared in THF/water (1:9, v/v) at pH 10 (0.1 mg/mL) one week after preparation.

In the basic aqueous solution of FpC_3NMe_2 after dialysis (Chapter 3.2), crystal-like solids were also observed. The solution was prepared by addition of 10.0 mL basic water (pH 12) into a THF solution of FpC_3NMe_2 (10.0 mg/mL, 1.0 mL) with a subsequent overnight dialysis. After being left quiescent for 10 days, some needle-like solids were found in the bottom of the vial.

The OM image of these precipitates suggests that their texture is close to transparent crystals (Figure 39).

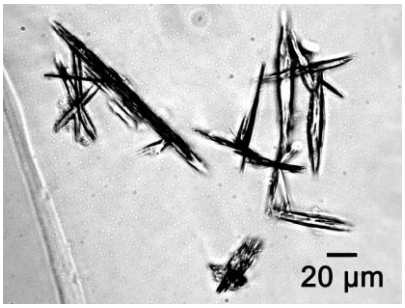

Figure 39. OM image of the needle-like crystals of FpC_3NMe_2 formed in the basic aqueous solution after dialysis and being left standing for 10 days (pH 12).

The needle-like crystals were found in the FpC_3NMe_2 solution prepared for the IR experiments as well (Chapter 3.4.3). The solution was prepared by fractional addition of 9.0 mL distilled water into a THF solution of FpC_3NMe_2 (28.0 mg/mL, 1.0 mL). When the solution was left standing for one day after the experiment, large amounts of thin and fragile needle-like precipitates were observed, as shown in Figure 40a. The OM image of these solids is displayed in Figure 40b, suggesting a transparent crystal-like structure.

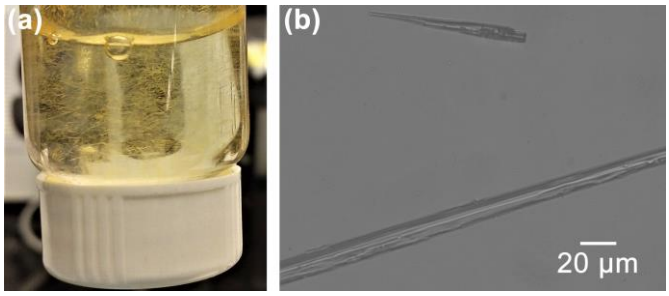

Figure 40. (a) Photograph; (b) OM image of the needle-like crystals of FpC_3NMe_2 formed in the THF/water solution one day after the IR experiment.

The above experiments demonstrate that, the FpC_3NMe_2 molecules can crystallize in either neutral or basic environments, but different pH, concentration, THF contents, and methods of the addition of the solvents will result in various morphologies of the crystals. The four conditions for crystallization are summarized in Table 1.

#	pH	Conc.	Preparation method	Stand time	Morphology of the crystals
1	10	0.1 mg/mL	Quick addition of 9.0 mL basic water into a THF solution of FpC_3NMe_2 (1.0 mg/mL, 1.0 mL)	At least 1 week	Flat rhombic
2	12				
3		1.0 mg/mL	Quick addition of 10.0 mL basic water into a THF solution of FpC_3NMe_2 (10.0 mg/mL, 1.0 mL), followed by dialysis		Needle-like
4	Neutral	2.8 mg/mL	Fractional addition of 9.0 mL distilled water into a THF solution of FpC_3NMe_2 (28.0 mg/mL, 1.0 mL)	Overnight	

Table 1. Different conditions for the crystallization of FpC_3NMe_2.

4. Conclusions

A new MC compound, FpC_3NMe_2 has been successfully synthesized. FpC_3NMe_2 molecules are non-surface active and hydrophobic, but can be hydrated in neutral water. Due to the protonation of the -NMe_2 groups, FpC_3NMe_2 can disperse in strong acid. At pH 1, FpC_3NMe_2 shows amphiphilic characteristics, despite its weaker surface activity and different behaviour from conventional surfactants. FpC_3NMe_2 colloids are unstable in THF/water solutions due to the protonation of -NMe_2 groups, which weakens the hydrophobic interaction between the chain tails and leads to irregular packing of the polarized Fp heads, eventually resulting in the disappearance of WCI after aggregation begins. In acidic THF/water solutions, FpC_3NMe_2 colloids are not stable as well. In some basic and neutral THF/water solutions, FpC_3NMe_2 solids are found to precipitate into crystals with different morphologies.

5. Future Work

Although TEM has been largely used in this study, no images can clearly illustrate the morphology of the prepared colloids. To solve this problem, cryo-TEM can be used, especially for those relatively stable colloids that are prepared at high temperature or in basic solutions.

At different pH environments, some interesting solution behaviour of FpC_3NMe_2 colloids in THF/water was observed. However, few studies have been conducted to interpret the principles behind this behaviour and the properties of the resulting assemblies. For example, AFM could be applied to study the lamellae formed at pH 3. The larger crystals could be analyzed by X-ray Diffraction (XRD) to obtain more detailed information about the FpC_3NMe_2 molecule, and this may also help to explain the unknown peaks appear in the NMR spectra.

Benefiting from WCI and the protonation of the $-NMe_2$ groups, better hydration property of FpC_3NMe_2 promises the possibility of its introduction into biological systems. Therefore, further investigation into its properties like biocompatibility is needed.

References

1. Bourrez, M.; Molton, F.; Chardon-Noblat, S.; Deronzier, A. *Angewandte Chemie* **2011,** 123, (42), 10077-10080.

2. Blum, Y.; Czarkie, D.; Rahamim, Y.; Shvo, Y. *Organometallics* **1985,** 4, (8), 1459-1461.

3. Kochi, J., *Organometallic mechanisms and catalysis: the role of reactive intermediates in organic processes*. Elsevier: **2012**.

4. Pacor, S.; Zorzet, S.; Cocchietto, M.; Bacac, M.; Vadori, M.; Turrin, C.; Gava, B.; Castellarin, A.; Sava, G. *Journal of Pharmacology and Experimental Therapeutics* **2004,** 310, (2), 737-744.

5. Schatzschneider, U.; Metzler-Nolte, N. *Angewandte Chemie International Edition* **2006,** 45, (10), 1504-1507.

6. Meister, K.; Niesel, J.; Schatzschneider, U.; Metzler-Nolte, N.; Schmidt, D. A.; Havenith, M. *Angewandte Chemie International Edition* **2010,** 49, (19), 3310-3312.

7. Motterlini, R.; Clark, J. E.; Foresti, R.; Sarathchandra, P.; Mann, B. E.; Green, C. J. *Circulation research* **2002,** 90, (2), e17-e24.

8. Clark, J. E.; Naughton, P.; Shurey, S.; Green, C. J.; Johnson, T. R.; Mann, B. E.; Foresti, R.; Motterlini, R. *Circulation research* **2003,** 93, (2), e2-e8.

9. Nobre, L. S.; Seixas, J. D.; Romão, C. C.; Saraiva, L. M. *Antimicrobial agents and chemotherapy* **2007,** 51, (12), 4303-4307.

10. Chandler, D. *Nature* **2005,** 437, (7059), 640.

11. Smith, R.; Baird, M. *Inorganica Chimica Acta* **1982,** 62, 135-139.

12. Schatzschneider, U. *British journal of pharmacology* **2015,** 172, (6), 1638-1650.

13. Gonzales, M. A.; Han, H.; Moyes, A.; Radinos, A.; Hobbs, A. J.; Coombs, N.; Oliver, S. R.; Mascharak, P. K. *Journal of Materials Chemistry B* **2014,** 2, (15), 2107-2113.

14. Nguyen, D.; Nguyen, T.-K.; Rice, S. A.; Boyer, C. *Biomacromolecules* **2015,** 16, (9), 2776-2786.

15. Berke, H.; Hoffmann, R. *Journal of the American Chemical Society* **1978,** 100, (23), 7224-7236.

16. Green, M.; Westlake, D. *Journal of the Chemical Society A: Inorganic, Physical, Theoretical* **1971**, 367-371.

17. Liu, J.; Cao, K.; Nayyar, B.; Tian, X.; Wang, X. *Polymer Chemistry* **2014,** 5, (23), 6702-6709.

18. Theys, R. D.; Dudley, M. E.; Hossain, M. M. *Coordination Chemistry Reviews* **2009,** 253, (1), 180-234.

19. Sharma, H. K.; Cervantes-Lee, F.; Pannell, K. H. *Journal of the American Chemical Society* **2004,** 126, (5), 1326-1327.

20. Cao, K.; Tsang, B.; Liu, Y.; Chelladural, D.; Power, W. P.; Wang, X. *Organometallics* **2014,** 33, (2), 531-539.

21. Wang, X.; Cao, K.; Liu, Y.; Tsang, B.; Liew, S. *Journal of the American Chemical Society* **2013,** 135, (9), 3399-3402.

22. Zhang, J.; Cao, K.; Wang, X.; Cui, B. *Chemical Communications* **2015,** 51, (99), 17592-17595.

23. Ye, W. N.; Xiong, Y. *Journal of Modern Optics* **2013,** 60, (16), 1299-1320.

24. Wiggins, P. M. *Physica A: Statistical Mechanics and its Applications* **1997,** 238, (1-4), 113-128.

25. Cheng, Y.-K.; Rossky, P. J. *Nature* **1998,** 392, (6677), 696.

26. Garde, S.; Hummer, G.; García, A. E.; Paulaitis, M. E.; Pratt, L. R. *Physical review letters* **1996,** 77, (24), 4966.

27. Davis, J. G.; Gierszal, K. P.; Wang, P.; Ben-Amotz, D. *Nature* **2012,** 491, (7425), 582.

28. Ashbaugh, H. S.; Truskett, T. M.; Debenedetti, P. G. *The Journal of chemical physics* **2002,** 116, (7), 2907-2921.

29. Zhang, S. *Nature biotechnology* **2003,** 21, (10), 1171.

30. Tanford, C., *The Hydrophobic Effect: Formation of Micelles and Biological Membranes 2d Ed*. J. Wiley.: **1980**.

31. Tateishi, Y.; Kai, N.; Noguchi, H.; Uosaki, K.; Nagamura, T.; Tanaka, K. *Polymer Chemistry* **2010,** 1, (3), 303-311.

32. De Jeu, W. *Molecular Physics* **1970,** 18, (1), 31-37.

33. Loh, T.-P.; Liung, S. B. K. W.; Tan, K.-L.; Wei, L.-L. *Tetrahedron* **2000,** 56, (20), 3227-3237.

34. Cowie, J. M.; Mohsin, M. A.; McEwen, I. J. *Polymer* **1987,** 28, (9), 1569-1572.

35. King, R. *Journal of the American Chemical Society* **1963,** 85, (13), 1918-1922.

36. Cao, K.; Murshid, N.; Li, L.; Lopez, A.; Tam, K. C.; Wang, X. *Macromolecules* **2015,** 48, (21), 7968-7977.

37. Murshid, N.; Wang, X. *Chemistry-A European Journal* **2015,** 21, (52), 19223-19230.

38. Murshid, N.; Wang, X. *The Journal of Physical Chemistry B* **2017,** 121, (25), 6280-6285.

39. Prabhu, R.; Shanbhag, A.; Venkatesha, T. *Journal of Applied Electrochemistry* **2007,** 37, (4), 491-497.

40. Alder, R.; Bowman, P.; Steele, W.; Winterman, D. *Chemical Communications (London)* **1968**, (13), 723-724.

41. Hibbert, F.; Hunte, K. P. *Journal of the Chemical Society, Perkin Transactions 2* **1983**, (9), 1895-1899.

42. Rizzo, R. C.; Jorgensen, W. L. *Journal of the American Chemical Society* **1999,** 121, (20), 4827-4836.

43. Loukonen, V.; Kurtén, T.; Ortega, I.; Vehkamäki, H.; Padua, A. A.; Sellegri, K.; Kulmala, M. *Atmospheric Chemistry and Physics* **2010,** 10, (10), 4961-4974.

44. Sesalan, B. Ş.; Koca, A.; Gül, A. *Dyes and Pigments* **2008,** 79, (3), 259-264.

45. Dai, S.; Ravi, P.; Tam, K. C.; Mao, B. W.; Gan, L. H. *Langmuir* **2003,** 19, (12), 5175-5177.

46. Li, Y.; Lokitz, B. S.; McCormick, C. L. *Angewandte Chemie International Edition* **2006,** 45, (35), 5792-5795.

47. Jeong, B.; Gutowska, A. *Trends in biotechnology* **2002,** 20, (7), 305-311.

48. Medeiros, S.; Santos, A.; Fessi, H.; Elaissari, A. *International journal of pharmaceutics* **2011,** 403, (1), 139-161.

49. Qin, S.; Geng, Y.; Discher, D. E.; Yang, S. *Advanced Materials* **2006,** 18, (21), 2905-2909.

50. Li, M.-H.; Keller, P. *Soft Matter* **2009,** 5, (5), 927-937.

51. Ahmed, F.; Discher, D. E. *Journal of controlled release* **2004,** 96, (1), 37-53.

52. Schmaljohann, D. *Advanced Drug Delivery Reviews* **2006,** 58, (15), 1655-1670.

53. Kurisawa, M.; Yokoyama, M.; Okano, T. *Journal of Controlled Release* **2000,** 69, (1), 127-137.

54. Bütün, V.; Armes, S.; Billingham, N. *Polymer* **2001,** 42, (14), 5993-6008.

55. Vamvakaki, M.; Billingham, N.; Armes, S. *Macromolecules* **1999,** 32, (6), 2088-2090.

56. Zhou, L.; Gao, C.; Xu, W. *Journal of Materials Chemistry* **2009,** 19, (31), 5655-5664.

57. Zhuravlev, L. T. *Langmuir* **1987,** 3, (3), 316-318.

58. Dou, L.; Chen, C.-C.; Yoshimura, K.; Ohya, K.; Chang, W.-H.; Gao, J.; Liu, Y.; Richard, E.; Yang, Y. *Macromolecules* **2013,** 46, (9), 3384-3390.

59. Wolf, C.; Lerebours, R. *The Journal of Organic Chemistry* **2003,** 68, (19), 7551-7554.

60. Wulff, W. D.; Peterson, G. A.; Bauta, W. E.; Chan, K.-S.; Faron, K. L.; Gilbertson, S. R.; Kaesler, R. W.; Yang, D. C.; Murray, C. K. *The Journal of Organic Chemistry* **1986,** 51, (2), 277-279.

61. Davoust, M.; Briere, J.-F.; Metzner, P. *Organic & Biomolecular Chemistry* **2006,** 4, (16), 3048-3051.

62. Nguyen, P.; Yuan, Z.; Agocs, L.; Lesley, G.; Marder, T. B. *Inorganica Chimica Acta* **1994,** 220, (1), 289-296.

63. Smithen, D. A.; Cameron, T. S.; Thompson, A. *Organic Letters* **2011,** 13, (21), 5846-5849.

64. Plotkin, J. S.; Shore, S. G. *Inorganic Chemistry* **1981,** 20, (1), 284-285.

65. Jiang, H.; Geng, D.; Liu, D.; Lanigan, N.; Wang, X. *Chemistry-A European Journal* **2017,** 23, (34), 8280-8285.

66. Gottlieb, H. E.; Kotlyar, V.; Nudelman, A. *The Journal of organic chemistry* **1997,** 62, (21), 7512-7515.

67. Bayliss, N. S.; McRae, E. G. *The Journal of Physical Chemistry* **1954,** 58, (11), 1006-1011.

68. Tonner, R.; Frenking, G. *Chemistry–A European Journal* **2008,** 14, (11), 3273-3289.

69. Shortt, A. B.; Durham, L. J.; Mosher, H. S. *The Journal of Organic Chemistry* **1983,** 48, (18), 3125-3126.

70. Binks, B. P. *Current opinion in colloid & interface science* **2002,** 7, (1), 21-41.

71. Oda, Y.; Horinouchi, A.; Kawaguchi, D.; Matsuno, H.; Kanaoka, S.; Aoshima, S.; Tanaka, K. *Langmuir* **2014,** 30, (5), 1215-1219.

72. Nuñez, N. O.; Morales, M. P.; Tartaj, P.; Serna, C. J. *Journal of Materials Chemistry* **2000,** 10, (11), 2561-2565.

73. Long, N. V.; Nogami, M.; Thi, C. M.; Ohtaki, M. *Journal of Advanced Microscopy Research* **2012,** 7, (2), 1-20.